# Interaction of wave with a body submerged below an ice sheet with multiple arbitrarily spaced cracks

Z. F. Li, G. X. Wu, and C. Y. Ji

Citation: Physics of Fluids **30**, 057107 (2018); doi: 10.1063/1.5030378
View online: https://doi.org/10.1063/1.5030378
View Table of Contents: http://aip.scitation.org/toc/phf/30/5
Published by the American Institute of Physics

# Interaction of wave with a body submerged below an ice sheet with multiple arbitrarily spaced cracks

Z. F. Li,[1] G. X. Wu,[1,2,a)] and C. Y. Ji[1]
[1]*School of Naval Architecture and Ocean Engineering, Jiangsu University of Science and Technology, Zhenjiang 212003, China*
[2]*Department of Mechanical Engineering, University College London, Torrington Place, London WC1E 7JE, United Kingdom*

(Received 21 March 2018; accepted 1 May 2018; published online 21 May 2018)

The problem of wave interaction with a body submerged below an ice sheet with multiple arbitrarily spaced cracks is considered, based on the linearized velocity potential theory together with the boundary element method. The ice sheet is modeled as a thin elastic plate with uniform properties, and zero bending moment and shear force conditions are enforced at the cracks. The Green function satisfying all the boundary conditions including those at cracks, apart from that on the body surface, is derived and is expressed in an explicit integral form. The boundary integral equation for the velocity potential is constructed with an unknown source distribution over the body surface only. The wave/crack interaction problem without the body is first solved directly without the need for source. The convergence and comparison studies are undertaken to show the accuracy and reliability of the solution procedure. Detailed numerical results through the hydrodynamic coefficients and wave exciting forces are provided for a body submerged below double cracks and an array of cracks. Some unique features are observed, and their mechanisms are analyzed. *Published by AIP Publishing.*
https://doi.org/10.1063/1.5030378

## I. INTRODUCTION

The physical behaviors of ocean waves in open water and icy regions are different. When free surface waves propagate into a region covered by an ice sheet, or the other way round, there will be wave reflection and transmission. In such a way, the wave/body interactions in icy waters can be expected to be much more complex than those in open waters.

When the horizontal dimension of the ice is much larger than its vertical one, it can be treated as an elastic plate based on the field measurements.[1] Through this model for a large ice sheet, a variety of work has been carried out to simulate and understand the wave propagation features in the polar regions. By using the matched eigenfunction expansions (MEE), Fox and Squire[2] constructed the solution for waves propagating from open water to a region below a semi-infinite ice sheet. The results showed that wave reflection would become stronger for a shorter wave. It was also found that there was a critical incident angle, larger than which, the waves would be totally reflected for any wave numbers. The unknowns in the eigenfunction expansions can be also solved through introducing an inner product of orthogonality, e.g., done by Sahoo, Yip, and Chwang[3] in which various ice edge conditions were examined. Other solution methods are also possible. Balmforth and Craster,[4] for example, solved the semi-infinite ice sheet problem using the Wiener-Hopf method. Furthermore, in that work, several non-dimensional parameters were introduced, through which it was found that the thin plate model could give nearly the same results as those by the Timoskenko-Mindlin model even for quite thick ice sheets. The ice sheet may not always be sufficiently large so that it can be treated as semi-infinite. There are also many cases in which the finite width of the ice sheet may have to be taken into account. Based on the solution for waves from open water to the semi-infinite ice sheet together with the Stokes time reverse, Meylan and Squire[5] constructed an approximate solution for waves propagating through an ice floe, the accuracy of which was verified by the exact solution constructed through the Green function method.[6] For an ice floe, it was found that there were a series of discrete frequencies at which the reflection coefficient was zero. Similar phenomenon could be also found in the polynya problem, e.g., in the work of Chung and Linton[7] where the solution was built via the residue calculus technique. A more general case was considered by Williams and Squire[8] through the Wiener-Hopf technique, i.e., the water surface was covered by three plates with different properties and the polynya could be treated with the thickness of the middle plate taken as zero.

In the above work, the ice sheet is assumed to be perfect. However, in many cases, the ice sheet may be imperfect, and one of such examples is the ice sheet with cracks. By following the MEE procedure in the work of Fox and Squire,[2] Barrett and Squire[9] solved the propagation of waves through an ice with a crack for finite water depth and found that there was a specific period at which perfect transmission would occur. Based on the Green function for an infinite homogeneous ice sheet, Squire and Dixon[10] obtained an analytical solution for infinite water depth, and the trend of the variation of reflection coefficient was found to be similar to that for finite water depth. The solution procedure was then extended to the problem for

[a)]Author to whom correspondence should be addressed: g.wu@ucl.ac.uk. Tel.: +44 20 7679 3870. Fax: +44 20 7388 0180.

the ice sheet with many cracks by Squire and Dixon,[11] and the results showed that perfect transmissions would occur at a discrete of periods. By first dividing the problem into the symmetric and anti-symmetric parts, Evans and Porter[12] found the analytical solution in the series form, for a single crack problem with finite water depth and an oblique incident wave. Specifically, the edge waves were found to be possible. Later, Porter and Evans[13] solved the problem of wave propagation through multiple cracks, and it was found that there were some stopping bands for the case with a semi-infinite array of cracks, within which the transmission coefficient was zero. Porter and Evans[14] also derived the solution for the ice sheet with finite length cracks.

In this work, we shall consider the problem of wave interaction with a body of arbitrary shape submerged below an ice sheet with multiple arbitrarily spaced cracks, which is an extension of the previous work by Li, Wu, and Ji[15] on a circular cylinder submerged below an ice sheet with the single crack problem through the analytical method. The multiple-crack problem has many practical applications. As noted by Squire and Dixon[11] or Porter and Evans,[13] for example, in the polar regions, there may be an area where the ice is fractured into floes that are presented at high concentrations, e.g., the shear zone that forms between moving and stationary sea ice.

It may be noticed that there have already been some studies on the coupled wave/body/ice interactions, motivated by development in the Arctic engineering. For an infinite homogeneous ice sheet, Li, Shi, and Wu[16] obtained the analytical solution for a circular cylinder undergoing large amplitude oscillations. By using the MEE, Sturova derived the Green function in a series form, for the cases of water surface covered by a semi-infinite ice sheet,[17] an infinite ice sheet with a crack,[18] and an ice floe or a polynya.[19] Through the Fourier transform technique, Li, Wu, and Ji[15] derived the Green function for the ice sheet with a crack in a simple integral form, and the multipoles for a submerged circular cylinder were further obtained. For a floating body on a polynya, Ren, Wu, and Thomas[20] obtained an analytical solution for a rectangle through MEE, and quite oscillatory behaviors of the hydrodynamic forces against the wave frequency have been observed. To solve the problem for a body of arbitrary shape, Li, Shi, and Wu[21] used the hybrid method which combined the eigenfunction expansion method and the boundary element method. When the gap between the body and the ice was large, the wide spacing approximation could be constructed, through which the mechanisms of the oscillatory features of the hydrodynamic forces could be uncovered.[22]

The paper is organized as follows. In Sec. II, the linearized boundary value problem for the velocity potential is presented, and the conditions at the cracks are described. In Sec. III A, the Green function satisfying all the boundary conditions except that on the body surface is first derived, based on which the velocity potential is solved in Sec. III B through the source distribution method, and the solution for pure wave/crack interaction problem is obtained in an explicit form in Sec. III C. Numerical results are presented and discussed in Sec. IV, and conclusions are drawn in Sec. V.

## II. MATHEMATICAL MODEL

We consider the interaction problem of a wave with a body submerged below an ice sheet with multiple arbitrarily spaced parallel cracks, as shown in Fig. 1. A Cartesian coordinate system $Oxyz$ is defined, with the $x$-axis along the undisturbed mean upper surface of the fluid, $z$-axis pointing vertically upwards, and $y$-axis being parallel to the cracks. The ice sheet with uniform properties is extended from $x = -\infty$ to $x = +\infty$. Its draught is assumed to be zero, and the $N$ parallel cracks are assumed to be located at $x = c_i$, $i = 1,2, \ldots, N$, with $c_i < c_{i+1}$, as shown in the figure.

The fluid with density $\rho$ and depth $H$ is assumed to be inviscid, incompressible, and homogeneous, and its motion is assumed to be irrotational. Under the assumption that the amplitude of the wave motion is small compared to its length and the dimension of the body, the linearized velocity potential theory can be used to describe the fluid flow. By further assuming that the motion is sinusoidal in time with radian frequency $\omega$, the total velocity potential $\Phi$ can be written in the following form:

$$\Phi(x,z,t) = \mathrm{Re}\left[\alpha_0\phi_0(x,z)\mathrm{e}^{\mathrm{i}\omega t} + \sum_{j=1}^{3}\mathrm{i}\omega\alpha_j\phi_j(x,z)\mathrm{e}^{\mathrm{i}\omega t}\right], \quad (1)$$

where $\phi_0$ contains the incident potential $\phi_I$ and diffracted potential $\phi_D$, $\alpha_0$ is the amplitude of the incident wave, and $\phi_j$ ($j$ = 1, 2, 3) is the radiation potential due to body oscillation with complex amplitude $\alpha_j$ in three degrees of freedom, i.e., translations in the $x$ and $z$ directions, respectively, and rotation about the $y$-axis pointing into the paper. Here a two-dimensional problem has been implied, and both the body

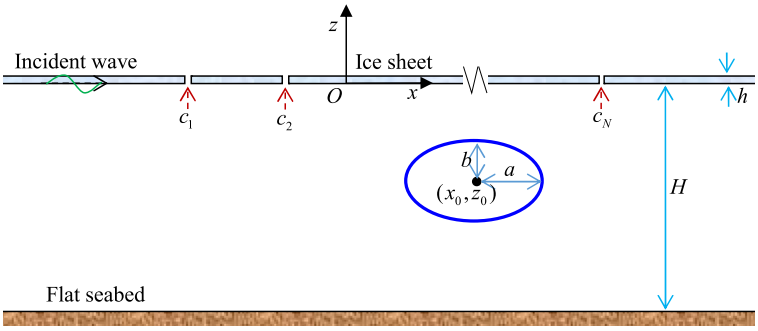


FIG. 1. Coordinate system and sketch of the problem.

and incoming wave are assumed to have the constant cross section in the $y$ direction.

Mass conservation requires that the potential $\phi_j$ satisfies Laplace's equation throughout the fluid or

$$\nabla^2\phi_j = 0, (j = 0,\ 1,\ 2,\ 3). \tag{2}$$

The ice sheet is modeled as a continuous elastic plate with uniform properties, i.e., thickness $h$, density $\rho_0$, Young's modulus $E$, and Poisson's ratio $\nu$ are all constant. Thus the boundary condition on the ice sheet can be given as

$$\left(L\frac{\partial^4}{\partial x^4} - m\omega^2 + \rho g\right)\frac{\partial\phi_j}{\partial z} - \rho\omega^2\phi_j = 0, (x \neq c_i, z = 0), \tag{3}$$

where $L = Eh^3/[12(1-\nu^2)]$ and $m = h\rho_0$ are the effective flexural rigidity and mass per unit area of the ice sheet. At the ice cracks, zero bending moment and shear force are assumed there, which gives

$$\frac{\partial^2}{\partial x^2}\left(\frac{\partial\phi_j}{\partial z}\right) = 0 \text{ and } \frac{\partial^3}{\partial x^3}\left(\frac{\partial\phi_j}{\partial z}\right) = 0, (x = c_i, z = 0). \tag{4}$$

The impermeable condition on the body surface can be written as

$$\frac{\partial\phi_0}{\partial n} = 0 \text{ and } \frac{\partial\phi_j}{\partial n} = n_j, (j = 1, 2, 3), \tag{5}$$

where $n_1$ and $n_2$ are, respectively, the $x$ and $z$ components of the unit normal vector $\vec{n}$ pointing into the body. $n_3 = (z-z')n_1 - (x-x')n_2$ is the component related to the rotational mode about $y$-axis, with $(x', z')$ as the rotational centre. Similarly, on the flat seabed, the following condition should also be enforced:

$$\frac{\partial\phi_j}{\partial z} = 0, (z = -H). \tag{6}$$

The radiation condition at infinity requires the wave to propagate outwards, i.e.,

$$\lim_{x\to\pm\infty}\left(\frac{\partial\phi_D}{\partial x} \pm i\lambda\phi_D\right) = 0 \text{ and } \lim_{x\to\pm\infty}\left(\frac{\partial\phi_j}{\partial x} \pm i\lambda\phi_j\right) = 0, \quad (j = 1, 2, 3), \tag{7}$$

where $\lambda$ is the purely positive real root of the following dispersion equation for a flexural gravity wave in the ice sheet:

$$K(\omega, \lambda) \equiv (L\lambda^4 + \rho g - m\omega^2)\lambda \tanh(\lambda H) - \rho\omega^2 = 0. \tag{8}$$

## III. SOLUTION PROCEDURES

### A. Velocity potential due to a single source: The Green function

The Green function $G(x, z; x_0, z_0)$ is defined as the velocity potential at point $p(x, z)$ due to a source at $q(x_0, z_0)$, which satisfies the following equation:

$$\nabla^2 G = 2\pi\delta(x - x_0)\delta(z - z_0), \tag{9}$$

throughout the fluid and the same boundary conditions as those in Eqs. (3), (4), (6), and (7). Here, $\delta(x)$ is the Dirac delta-function.

By following the procedure in the work of Li, Wu, and Ji[15] who derived the Green function for an ice sheet with a single crack in an integral form, $G$ for multiple parallel cracks can be written as

$$G = G_{ice}(x, z; x_0, z_0) + \sum_{i=1}^{N}\left[A_{N,i}\frac{\partial G_1(x - c_i, z)}{\partial x} + B_{N,i}G_1(x - c_i, z)\right], \tag{10}$$

where

$$G_{ice} = \ln\left(\frac{r_1}{H}\right) + \ln\left(\frac{r_2}{H}\right) - 2\int_D \frac{e^{-kH}}{k}\{P(k)Z(z)Z(z_0)\cos[k(x - x_0)] + 1\}dk \tag{11}$$

and

$$G_1(x, z) = \frac{L}{\pi}\int_D \frac{Z(z)}{K(\omega, k)Z(0)}k^2\cos(kx)dk, \tag{12}$$

with

$$Z(z) = \cosh[k(z + H)] \tag{13}$$

and

$$P(k) = \frac{(Lk^4 + \rho g - m\omega^2)k + \rho\omega^2}{K(\omega, k)Z(0)}. \tag{14}$$

Here $r_1$ is the distance between $p$ and $q$ and $r_2$ is the distance between $p$ and the mirror image of $q$ about the flat seabed $z = -H$. To satisfy the radiation condition at infinity, the integration route $D$ in $G_{ice}$ and $G_1$ from 0 to $+\infty$ should pass over the pole at $k = \lambda$. $G_{ice}$ in Eq. (10) is in fact the Green function without cracks. Each pair of the terms in the square brackets corresponds to each crack, and $A_{N,i}$ and $B_{N,i}$ represent the jumps of the displacement and the slope on both sides of the crack. Thus at $x = c_i$,

$$\left(\frac{\partial G}{\partial z}\right)_{x=c_i^+}^{x=c_i^-} = A_{N,i}(x_0, z_0), (z = 0), \tag{15}$$

$$\left(\frac{\partial^2 G}{\partial z\partial x}\right)_{x=c_i^+}^{x=c_i^-} = B_{N,i}(x_0, z_0), (z = 0). \tag{16}$$

It may be noticed that $G_1$ and $G_{ice}$ can be related through the following equation:[15]

$$G_1(x, z) = \frac{L}{2\pi\rho\omega^2}\left[\frac{\partial^3 G_{ice}(x_0, z_0; x, z)}{\partial z_0\partial x_0^2}\right]_{x_0=0, z_0=0}. \tag{17}$$

The summation in Eq. (10) involving $G_1$ is introduced to satisfy the conditions in Eq. (4) at each crack, which can be used to determine the two sets of unknown coefficients $A_{N,i}$ and $B_{N,i}$. Thus at the crack of $x = c_j$, we have

$$\lim_{\substack{z\to 0\\ x\to c_j}} G_{zxx} = \frac{2\pi\rho\omega^2}{L}[G_1(x - x_0, z_0)]_{x=c_j} + \lim_{\substack{z\to 0\\ x\to c_j}}\sum_{i=1}^{N}\left[A_{N,i}\frac{\partial^4 G_1(x - c_i, z)}{\partial z\partial x^3} + B_{N,i}\frac{\partial^3 G_1(x - c_i, z)}{\partial z\partial x^2}\right] = 0 \tag{18}$$

and

$$\lim_{\substack{z\to 0\\ x\to c_j}} G_{zxx} = \frac{2\pi\rho\omega^2}{L}\left[\frac{\partial G_1(x-x_0,z_0)}{\partial x}\right]_{x=c_j} + \lim_{\substack{z\to 0\\ x\to c_j}} \sum_{i=1}^{N}\left[A_{N,i}\frac{\partial^5 G_1(x-c_i,z)}{\partial z\partial x^4} + B_{N,i}\frac{\partial^4 G_1(x-c_i,z)}{\partial z\partial x^3}\right] = 0, \tag{19}$$

in which Eq. (17) has been used. Similar to that in the work of Li, Wu, and Ji,[15] we have

$$I^1_{N,ji} = \lim_{\substack{z\to 0\\ x\to c_j}} \frac{\partial^3 G_1(x-c_i,z)}{\partial z\partial x^2} = -\frac{1}{\pi}\int_D \frac{\rho\omega^2-(\rho g-m\omega^2)k\,\tanh(kH)}{K(\omega,k)}\cos[k(c_j-c_i)]\mathrm{d}k, \tag{20}$$

$$I^2_{N,ji} = \lim_{\substack{z\to 0\\ x\to c_j}} \frac{\partial^4 G_1(x-c_i,z)}{\partial z\partial x^3} = \frac{1}{\pi}\int_D \frac{\rho\omega^2-(\rho g-m\omega^2)k\,\tanh(kH)}{K(\omega,k)}k\,\sin[k(c_j-c_i)]\mathrm{d}k, \tag{21}$$

$$I^3_{N,ji} = \lim_{\substack{z\to 0\\ x\to c_j}} \frac{\partial^5 G_1(x-c_i,z)}{\partial z\partial x^4} = \frac{1}{\pi}\int_D \frac{\rho\omega^2-(\rho g-m\omega^2)k\,\tanh(kH)}{K(\omega,k)}k^2\cos[k(c_j-c_i)]\mathrm{d}k. \tag{22}$$

It may be noticed that here we have $I^1_{N,ji} = I^1_{N,ij}$ and $I^1_{N,ii} = I^1_{N,11}$, $I^2_{N,ji} = -I^2_{N,ij}$, $I^3_{N,ji} = I^3_{N,ij}$, and $I^3_{N,ii} = I^3_{N,11}$. Substituting Eqs. (20)–(22) into Eqs. (18) and (19) at each ice crack of $x = c_j$ ($j$ = 1,2, . . ., $N$), we can obtain totally $2N$ equations. Thus the two set of unknown coefficients $A_{N,i}$ and $B_{N,i}$ with $i$ = 1,2, . . ., $N$ can be found through a matrix equation $\mathbf{H}\cdot\boldsymbol{A} = \boldsymbol{U}$ or

$$\begin{bmatrix} 0 & \cdots & I^2_{N,1N} & I^1_{N,11} & \cdots & I^1_{N,1N}\\ \vdots & \ddots & \vdots & \vdots & \ddots & \vdots\\ I^2_{N,N1} & \cdots & 0 & I^1_{N,N1} & \cdots & I^1_{N,NN}\\ I^3_{N,11} & \cdots & I^3_{N,1N} & 0 & \cdots & I^2_{N,1N}\\ \vdots & \ddots & \vdots & \vdots & \ddots & \vdots\\ I^3_{N,N1} & \cdots & I^3_{N,NN} & I^2_{N,N1} & \cdots & 0 \end{bmatrix}\begin{Bmatrix} A_{N,1}\\ \vdots\\ A_{N,N}\\ B_{N,1}\\ \vdots\\ B_{N,N}\end{Bmatrix} = \begin{Bmatrix} U_{N,1}\\ \vdots\\ U_{N,N}\\ V_{N,1}\\ \vdots\\ V_{N,N}\end{Bmatrix}, \tag{23}$$

where

$$U_{N,j}(x_0,z_0) = -\frac{2\pi\rho\omega^2}{L}[G_1(x-x_0,z_0)]_{x=c_j}, \tag{24}$$

$$V_{N,j}(x_0,z_0) = -\frac{2\pi\rho\omega^2}{L}\left[\frac{\partial G_1(x-x_0,z_0)}{\partial x}\right]_{x=c_j}. \tag{25}$$

From Eq. (23), we can obtain $\boldsymbol{A} = \mathbf{H}^{-1}\cdot\boldsymbol{U}$. It may be noticed that the matrix $\mathbf{H}$ depends on only the relative positions of the ice cracks and is independent of the source position. Therefore, $\mathbf{H}^{-1}$ can be computed in advance and is valid for any location of the source point. We may assume that $C_{ij}$ are the coefficients of $\mathbf{H}^{-1}$, which provides

$$A_{N,i} = \sum_{j=1}^{N} C_{ij}U_{N,j} + \sum_{j=1}^{N} C_{i(j+N)}V_{N,j}, \tag{26}$$

$$B_{N,i} = \sum_{j=1}^{N} C_{(i+N)j}U_{N,j} + \sum_{j=1}^{N} C_{(i+N)(j+N)}V_{N,j}. \tag{27}$$

Substituting Eqs. (26) and (27) into Eq. (10) and noticing

$$[G_1(x-x_0,z_0)]_{x=c_j} = [G_1(x_0-x,z_0)]_{x=c_j}, \tag{28}$$

$$\left[\frac{\partial G_1(x-x_0,z_0)}{\partial x}\right]_{x=c_j} = -\left[\frac{\partial G_1(x_0-x,z_0)}{\partial x_0}\right]_{x=c_j}, \tag{29}$$

we can obtain

$$G = G_{ice}(x,z;x_0,z_0) + \frac{2\pi\rho\omega^2}{L}\sum_{i=1}^{N}\sum_{j=1}^{N}\left\{\left[C_{i(j+N)}\frac{\partial G_1(x-c_i,z)}{\partial x}\frac{\partial G_1(x_0-c_j,z_0)}{\partial x_0} - C_{(i+N)j}G_1(x-c_i,z)G_1(x_0-c_j,z_0)\right] + \left[C_{(i+N)(j+N)}G_1(x-c_i,z)\frac{\partial G_1(x_0-c_j,z_0)}{\partial x_0} - C_{ij}\frac{\partial G_1(x-c_i,z)}{\partial x}G_1(x_0-c_j,z_0)\right]\right\}. \tag{30}$$

It can be shown (see Appendix A) that for $G(x, z; x_0, z_0)$, $(x, z)$ and $(x_0, z_0)$ are exchangeable. This together with Eq. (30) indicates that

$$C_{i(j+N)} = C_{j(i+N)}, C_{(i+N)j} = C_{(j+N)i}, C_{ij} = -C_{(j+N)(i+N)}, \tag{31}$$

which can also be obtained from the symmetric and skew symmetric natures of the sub matrixes of $\mathbf{H}$.

### B. Solution through the source distribution method

As shown in Appendix B, the velocity potential at $p(x, z)$ in the fluid can be expressed through a source distribution $\sigma_j(x, z)$ over the body surface $S_B$ only or

$$\phi_j(x,z) = \int_{S_B}\sigma_j(x_0,z_0)G(x,z;x_0,z_0)\mathrm{d}S, \tag{32}$$

and no source distribution is needed on other surfaces. We may notice that the integration is carried out with respect to $(x_0, z_0)$, and the velocity potential $\phi_j(x, z)$ satisfies all the boundary conditions apart from that on the body surface, which will be used to determine the source distribution $\sigma_j(x_0, z_0)$. To do that, we differentiate both sides of Eq. (32) with respect to the normal direction at $p \in S_B$ or

$$\frac{\partial \phi_j(x,z)}{\partial n_p} = -\alpha(x,z)\sigma_j(x,z) + \int_{S_B} \sigma_j(x_0,z_0)\frac{\partial G(x,z;x_0,z_0)}{\partial n_p}\mathrm{d}S, \tag{33}$$

where $\alpha$ is the solid angle at $(x, z)$.

For the radiation problem, $\partial\phi_j/\partial n = n_j$ can be used directly in Eq. (33). However, for the diffraction problem, we should first divide $\phi_D$ into two parts:

$$\phi_D = \phi_D^1 + \phi_D^2, \tag{34}$$

where $\phi_D^1$ is the diffraction potential by the cracks to $\phi_I$ and $\phi_D^2$ is that by the body to $\varphi = \phi_I + \phi_D^1$. When the incident wave propagates from $x = -\infty$ to $x = +\infty$, $\phi_I$ can be written in the following form:

$$\phi_I = I\mathrm{e}^{-\mathrm{i}\lambda x}\frac{\cosh[\lambda(z+H)]}{\cosh(\lambda H)}, \tag{35}$$

with $I = g/\mathrm{i}\omega$. As in the work of Li, Wu, and Ji,[15] applying Green's second identity to $\phi_D^1$ and $G$ in Eq. (10) over the fluid boundary $S$, we obtain

$$2\pi\phi_D^1(x,z) = \int_S \left[\phi_D^1(x_0,z_0)\frac{\partial G(x,z;x_0,z_0)}{\partial n_q} - G(x,z;x_0,z_0)\frac{\partial \phi_D^1(x_0,z_0)}{\partial n_q}\right]\mathrm{d}S, \tag{36}$$

where the derivative and integration are carried out with respect to $(x_0, z_0)$. Invoking the boundary conditions for $\phi_D^1$ and $G$, only the ice sheet will remain on the right hand side of Eq. (36). Using the condition in Eq. (3) and through integrating by parts, Eq. (36) can be further given as

$$2\pi\phi_D^1(x,z) = \frac{L}{\rho\omega^2}\sum_{i=1}^{N}\left[\left(\frac{\partial^4\phi_D^1}{\partial x_0^3\partial z_0}\frac{\partial G}{\partial z_0} - \frac{\partial^3\phi_D^1}{\partial x_0^2\partial z_0}\frac{\partial^2 G}{\partial x_0\partial z_0}\right)_{x_0=c_i^+}^{x_0=c_i^-}\right]_{z_0=0}. \tag{37}$$

Substituting Eqs. (15) and (16) into the above equation and noticing that $\varphi = \phi_I + \phi_D^1$ should satisfy the crack conditions in Eq. (4), $\phi_D^1$ in Eq. (37) can be given as

$$\phi_D^1(x,z) = -\frac{IL\lambda^3}{2\pi\rho\omega^2}\tanh(\lambda H) \times \sum_{j=1}^{N}\mathrm{e}^{-\mathrm{i}\lambda c_i}\left[\mathrm{i}\lambda A_{N,i}(x,z) + B_{N,i}(x,z)\right]. \tag{38}$$

By further applying Eqs. (26) and (27) to the above equation, we can obtain

$$\phi_D^1(x,z) = -I\lambda^3\tanh(\lambda H)\sum_{i=1}^{N}\sum_{j=1}^{N}\mathrm{e}^{-\mathrm{i}\lambda c_i} \times\left\{\left[\mathrm{i}\lambda C_{i(j+N)} + C_{(i+N)(j+N)}\right]\frac{\partial G_1(x-c_j,z)}{\partial x} - \left[\mathrm{i}\lambda C_{ij} + C_{(i+N)j}\right]G_1(x-c_j,z)\right\}. \tag{39}$$

As $\varphi = \phi_I + \phi_D^1$ satisfies the conditions at the crack, $\phi_D^2$ then should also satisfy these conditions. Thus we can apply Eq. (33) to $\phi_D^2$ by using $\partial\phi_D^2/\partial n = -\partial\varphi/\partial n$ on the body surface.

### C. Reflection and transmission coefficients for wave/crack interaction

Invoking Eq. (39), we can also obtain the reflection and transmission coefficients explicitly for a wave propagating across the cracks. Letting $x \to \pm\infty$ and by applying the Fourier integrals Eq. (13.16) in the work of Wehausen and Laitone[23] to the right hand sides of Eqs. (28) and (29), we have

$$\lim_{x\to\pm\infty} G_1(x-c_j,z) = -\mathrm{i}L\frac{\lambda^2\mathrm{e}^{\pm\mathrm{i}\lambda c_j}}{K'(\omega,\lambda)}\mathrm{e}^{\mp\mathrm{i}\lambda x}\frac{\cosh[\lambda(z+H)]}{\cosh(\lambda H)}, \tag{40}$$

$$\lim_{x\to\pm\infty}\frac{\partial G_1(x-c_j,z)}{\partial x} = \mp L\frac{\lambda^3\mathrm{e}^{\pm\mathrm{i}\lambda c_j}}{K'(\omega,\lambda)}\mathrm{e}^{\mp\mathrm{i}\lambda x}\frac{\cosh[\lambda(z+H)]}{\cosh(\lambda H)}. \tag{41}$$

From these two equations together with Eqs. (39) and (35), the asymptotic expression of the potential $\varphi$ can be given as

$$\varphi(x,z) = \begin{cases} I\times T_c\mathrm{e}^{-\mathrm{i}\lambda x}\dfrac{\cosh[\lambda(z+H)]}{\cosh(\lambda H)}, & x\to+\infty \\ I\left(\mathrm{e}^{-\mathrm{i}\lambda x} + R_c\mathrm{e}^{+\mathrm{i}\lambda x}\right)\dfrac{\cosh[\lambda(z+H)]}{\cosh(\lambda H)}, & x\to-\infty \end{cases}, \tag{42}$$

where $T_c$ and $R_c$ are, respectively, the transmission and reflection coefficients. Substituting Eqs. (40) and (41) into Eq. (39), we can obtain

$$T_c = 1 - L\lambda^5\frac{\tanh(\lambda H)}{K'(\omega,\lambda)}\sum_{i=1}^{N}\sum_{j=1}^{N}\mathrm{e}^{-\mathrm{i}\lambda(c_i-c_j)} \times\left[\mathrm{i}C_{(i+N)j} - \mathrm{i}\lambda^2 C_{i(j+N)} - \lambda C_{ij} - \lambda C_{(i+N)(j+N)}\right], \tag{43}$$

$$R_c = -L\lambda^5\frac{\tanh(\lambda H)}{K'(\omega,\lambda)}\sum_{i=1}^{N}\sum_{j=1}^{N}\mathrm{e}^{-\mathrm{i}\lambda(c_i+c_j)} \times\left[\mathrm{i}C_{(i+N)j} + \mathrm{i}\lambda^2 C_{i(j+N)} - \lambda C_{ij} + \lambda C_{(i+N)(j+N)}\right]. \tag{44}$$

Invoking Eq. (31), Eqs. (43) and (44) can be also given as

$$T_c = 1 - 2\mathrm{i}L\lambda^5\frac{\tanh(\lambda H)}{K'(\omega,\lambda)}\sum_{i=1}^{N}\sum_{j=i}^{N}h_{ij}\Big\{\cos\left[\lambda(c_i-c_j)\right] \times\left[C_{(i+N)j} - \lambda^2 C_{i(j+N)}\right] - \lambda\sin\left[\lambda(c_i-c_j)\right](C_{ji} - C_{ij})\Big\}, \tag{45}$$

$$R_c = -L\lambda^5\frac{\tanh(\lambda H)}{K'(\omega,\lambda)}\sum_{i=1}^{N}\sum_{j=i}^{N}\mathrm{e}^{-\mathrm{i}\lambda(c_i+c_j)}h_{ij} \times\left[\mathrm{i}C_{(i+N)j} + \mathrm{i}\lambda^2 C_{i(j+N)} - \lambda C_{ij} - \lambda C_{ji}\right], \tag{46}$$

where $h_{ij} = 1$ if $i = j$ and $h_{ij} = 2$ if $i \neq j$. It may be noticed that $T_c$ and $R_c$ should satisfy the energy balance equation[9] or

$$|T_c|^2 + |R_c|^2 = 1. \tag{47}$$

### D. Hydrodynamic force

After the velocity potentials have been found, the pressure can be obtained through the linear Bernoulli equation. Integrating the dynamic pressure over the mean wetted body surface, the hydrodynamic force then can be obtained. For the radiation potential, we have

$$\tau_{ij} = \mu_{ij} - \mathrm{i}\frac{\lambda_{ij}}{\omega} = \rho \int_{S_B} \phi_j n_i \mathrm{d}S, \tag{48}$$

where $\mu_{ij}$ and $\lambda_{ij}$ are, respectively, the added mass and damping coefficient. For the diffraction potential, we have

$$f_{E,i} = -\mathrm{i}\omega\rho \int_{S_B} \phi_0 n_i \mathrm{d}S, \tag{49}$$

where $f_{E,i}$ is the wave exciting force due to the incident potential $\phi_I$ with unit amplitude and its diffraction.

## IV. NUMERICAL RESULTS

### A. Wave propagation across the cracks without the body

We first consider the case of a wave propagating across the cracks without the body. This has been studied previously by Porter and Evans[13] through introducing a pair of canonical single crack functions $\psi_1$ and $\psi_2$ for a source located at the crack, which can be related to $G_1$ and $\partial G_1/\partial x$ in Eq. (10) as follows:

$$\psi_1(x,z) = -\frac{1}{\rho g} G_1(x,z), \psi_2(x,z) = -\frac{1}{\rho g}\frac{\partial G_1(x,z)}{\partial x}, \tag{50}$$

after the typos in their Eq. (2.29) are corrected. To carry out the comparisons, the parameters are chosen as $E$ = 5 GPa, $\nu = 0.3$, $h = 1$ m, $\rho_0 = 925$ kg/m$^3$, $\rho = 1025$ kg/m$^3$, $g = 9.81$ m/s$^2$, and $H = 40$ m, which are the same as those in the work of Porter and Evans.[13] The modulus of the transmission coefficient $|T_c|$ is plotted in Fig. 2, against the dimensionless wave number $\lambda h$, for two cracks or $N = 2$. Two different distances between the cracks are considered, with $c_2 = -c_1 = 20h$ and $c_2 = -c_1 = 0.25h$, respectively, and the results are shown in Figs. 2(a) and 2(b), respectively. The energy balance equation Eq. (47) has been used to check the accuracy of results. It can be seen from the figure that there is no visible difference between the present results and those given by Porter and Evans.[13] This verifies the present formulation and numerical procedure.

Compared with Fig. 2(b), we can observe from Fig. 2(a) that when the two cracks are more widely spaced, $|T_c|$ shows a quite oscillatory behavior with respect to $\lambda h$. When the spacing between the two cracks is large, we may take into account only the traveling wave components generated by each crack as in the wide polynya problem[22] and ignore those evanescent modes. We assume that the reflection and transmission coefficients for a single crack at the origin are $R$ and $T$, respectively. Let $l = c_2 - c_1$. When the incident wave of $I_0 = I\mathrm{e}^{-\mathrm{i}\lambda c_1}$ in Eq. (35) from $x = -\infty$ passes the first crack at $x = c_1$, it will arrive at the second crack at $x = c_2$ and then be reflected back to the first crack at $x = c_1$ as an incident wave from the right, with

$$I_1 = (I\mathrm{e}^{-\mathrm{i}\lambda c_1})(T\mathrm{e}^{-\mathrm{i}\lambda l})(R\mathrm{e}^{-\mathrm{i}\lambda l}). \tag{51}$$

Here the term in the second parenthesis reflects the effective incident wave to the second crack, which is reflected through $R$ and then travels back to crack one over a distance $l$. $I_1$ then contributes to the reflection and transmission of crack one as

$$R_1 = T \times I_1, \quad T_1 = R \times I_1. \tag{52}$$

The wave of $T_1$ above will then travel to crack two again and then return back to crack one. Following the same argument, we have

$$I_2 = T_1 \times R\mathrm{e}^{-2\mathrm{i}\lambda l}, \quad R_2 = T \times I_2, \quad T_2 = R \times I_2. \tag{53}$$

It is then obvious that

$$I_n = T_{n-1} \times R\mathrm{e}^{-2\mathrm{i}\lambda l}, \quad R_n = T \times I_n, \quad T_n = R \times I_n. \tag{54}$$

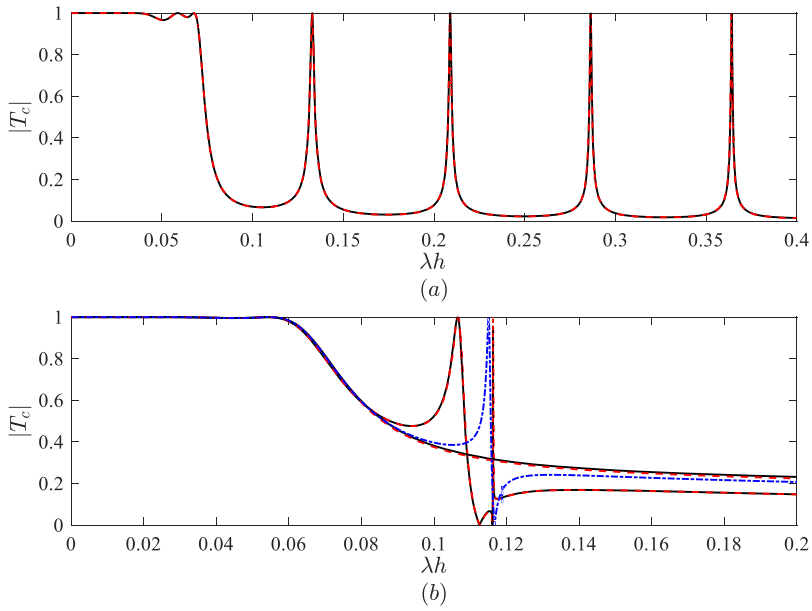


FIG. 2. Modulus of the transmission coefficient $|T_c|$ for wave propagation across two cracks. (a) $c_2 = -c_1 = 20h$ and (b) $c_2 = -c_1 = 0.25h$. Solid lines: results computed by the present method; dashed lines: results given in Porter and Evans.[13] The dotted-dashed line in (b) is for $c_2 = -c_1 = 0.05h$.

From this, $I_n$ can be written as

$$I_n = I_{n-1} \times R^2 e^{-2i\lambda l} = \frac{T}{R}(Ie^{-i\lambda c_1})(R^2 e^{-2i\lambda l})^n, \quad (55)$$

which provides

$$R_n = \frac{T^2}{R}\left(Ie^{-i\lambda c_1}\right)\left(R^2 e^{-2i\lambda l}\right)^n, \quad (56)$$

$$T_n = T\left(Ie^{-i\lambda c_1}\right)\left(R^2 e^{-2i\lambda l}\right)^n. \quad (57)$$

It may be noticed that although Eq. (55) is valid for $n \geq 2$, Eq. (56) is correct for $n \geq 1$, while Eq. (57) is correct for $n \geq 0$. From Eq. (56) and noticing the definition of $R_c$ in Eq. (42), we have

$$\begin{aligned} R_c &= e^{-2i\lambda c_1}\left[R + \frac{T^2}{R}\sum_{n=1}^{\infty}\left(R^2 e^{-2i\lambda l}\right)^n\right] \\ &= e^{-2i\lambda c_1}\left[R + \frac{RT^2 e^{-2i\lambda l}}{1 - R^2 e^{-2i\lambda l}}\right]. \end{aligned} \quad (58)$$

Similarly, from Eq. (57), we have

$$T_c = Te^{+i\lambda c_1}\left[T\left(Ie^{-i\lambda c_1}\right)\sum_{n=0}^{\infty}\left(R^2 e^{-2i\lambda l}\right)^n\right] = \frac{T^2}{1 - R^2 e^{-2i\lambda l}}. \quad (59)$$

The above equations may be also obtained by matching the travelling wave from $x = c_1$ to the right and that from $x = c_2$ to the left, as in the wide polynya problem.[22] Then similar to Li, Shi, and Wu,[22] it can be shown from Eq. (58) that $|R_c|$ will reach its peaks and troughs, respectively, when

$$\lambda l = n\pi - \pi/2 + \mathrm{Arg}(R) \quad (60)$$

and

$$\lambda l = n\pi + \mathrm{Arg}(R), \quad (61)$$

which, respectively, correspond to the troughs and peaks of $|T_c|$ based on Eq. (59). Here $n$ is an integer which ensures $\lambda > 0$, and Arg indicates the argument of the complex number. In particular, when Eq. (61) is satisfied, $|R_c| = 0$ and $|T_c| = 1$. It should be pointed out that the value of Arg($R$) for a single crack depends on the location of the crack or the relative horizontal location of $x = 0$ to the crack. When the horizontal location of the origin of the coordinate system is chosen differently, the value of Arg($R$) will be different. Accordingly the results on the right hand sides of Eqs. (60) and (61) will be different. However, what is more important here is how these results vary with $n$, which is not affected by Arg($R$). It may be also interesting to link Eqs. (60) and (61) with the natural sloshing modes of a rectangular tank (e.g., Ref. 24). In fact, the former is virtually the same as that for the odd mode and the latter for the even mode.

We may investigate the travelling wave between the two cracks. Invoking Eq. (57), we have the wave transmitting from crack one and propagating along the $x$-axis as

$$w_T = e^{-i\lambda(x-c_1)}\left[T\left(Ie^{-i\lambda c_1}\right)\sum_{n=0}^{\infty}\left(R^2 e^{-2i\lambda l}\right)^n\right] = \frac{ITe^{-i\lambda x}}{1 - R^2 e^{-2i\lambda l}}. \quad (62)$$

Similarly, the wave reflected by crack two and travelling in the opposite direction can be written as

$$w_R = \frac{IRTe^{-i\lambda l}e^{+i\lambda x}}{1 - R^2 e^{-2i\lambda l}}, \quad (63)$$

where $2c_2 = l$ has been used. Invoking Eqs. (62) and (63), we have

$$w = w_T + w_R = IT\frac{e^{-i\lambda x} + |R|e^{-i[\lambda l - \mathrm{Arg}(R)]}e^{+i\lambda x}}{1 - |R|^2 e^{-2i[\lambda l - \mathrm{Arg}(R)]}}. \quad (64)$$

It is known that for the wave propagating through a single crack, there exists one $\lambda h$ at which $|R| = 0$ (e.g., Ref. 12). This together with Eq. (64) indicates that there may be only the wave propagating to the positive $x$-axis at this special wave number. Invoking Eq. (47), we also have that $|R| < 1$, and when $|R| = 1$, $|T| = 0$. This together with Eq. (64) indicates that there will be no exact standing wave between two cracks.

From Fig. 2(b), we can see that the results for two narrowly spaced cracks follow more closely the pattern of a single crack. It is particularly the case at a long wave, in which the gap between the cracks becomes smaller relative to the wavelength. As $\lambda h$ further increases, it can be seen that except the sharp spikes within the range of $\lambda h \in (0.1, 0.12)$, $|T_c|$ follows the same pattern as that for a single crack. However, they are not the same, as the gap is no longer small relative to the wavelength. To see the trend when the gap decreases, the result is also provided in Fig. 2(b) for $c_2 = -c_1 = 0.05h$, and its curve is much closer to that of a single crack apart from a single point at which the result changes rapidly. The reason for the rapid variation of $|T_c|$ at this particular frequency has been discussed by Porter and Evans.[13]

### B. Body submerged below an ice sheet with two cracks

To solve Eq. (33) numerically, the body surface $S_B$ is divided into $N_B$ straight line segments. On each segment, the source strength $\sigma_j$ is assumed to be constant and the discretized equation is enforced at the centre of the element, which means that the solid angle $\alpha$ in Eq. (33) can always be taken as $\pi$. In this section and Sec. IV C, the numerical results are presented in the dimensionless form, based on a characteristic length scale, density of water $\rho = 1025\ \mathrm{kg\ m^{-3}}$, and acceleration due to gravity $g = 9.80\ \mathrm{ms^{-2}}$. When it is not specifically specified, the properties of the ice sheet are taken as

$$E = 5\,\mathrm{GPa},\ \nu = 0.3,\ \rho_0 = 922.5\,\mathrm{kg\,m^{-3}},\ h = 1\,\mathrm{m},\ H = 100\,\mathrm{m}, \quad (65)$$

which are similar to those in the work of Sturova[19] to provide physically meaningful results. The considered body will be an ellipse or $(x - x')^2/a^2 + (z - z')^2/b^2 = 1$, where $a$ and $b$ are the half axes of the body in the $x$ and $z$ directions, respectively. The rotational centre is taken to be at the geometric centre of the body or $(x', z')$, and $a$ is chosen as the characteristic length for nondimensionalisation. Unless specified, the numerical results are obtained by dividing the body surface into

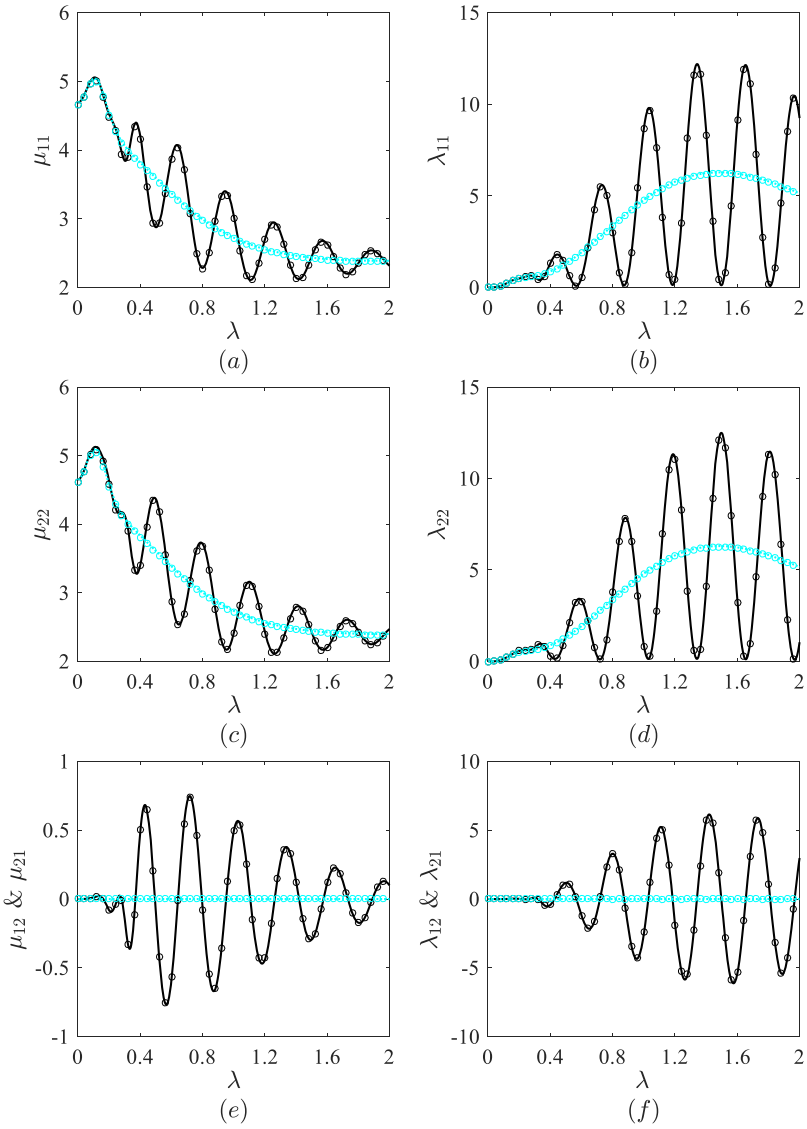


FIG. 3. Hydrodynamic coefficients of a submerged circular cylinder with a single crack on the left. Solid lines: $c_1 = -10$; dotted lines: ice sheet without crack. Open circles: analytical solutions based on the multipole expansion. ($a = 1$, $b = 1$, $x' = 0$, $z' = -1.2$, $H = 20$, $h = 0.2$, $m = 0.18$, $L = 72.932$).

$N_B = 240$ straight line segments, from which convergence has been achieved.

Here, we shall first consider wave interaction with a circular cylinder or $a = b$ submerged below an ice sheet, with a single crack on the left side of the body. Results are provided for $c_1 = -10$. The computed hydrodynamic coefficients are shown in Fig. 3, against the dimensionless wave number $\lambda$, while the corresponding wave exciting force is presented in Fig. 4. Only nonzero results are given as the rotation of a circular cylinder about its centre will not disturb the fluid. Similar to the procedure in Appendix A in the work of Li, Wu, and Ji,[15] it can be shown that $\tau_{ij} = \tau_{ji}$, i.e., $\mu_{ij}$ and $\lambda_{ij}$ given by Eq. (48) are symmetric. Thus only one of them is plotted in the figure. The results from analytical solutions based on multipole expansions[15] are also provided in each figure for comparison. It can be seen from these figures that there is

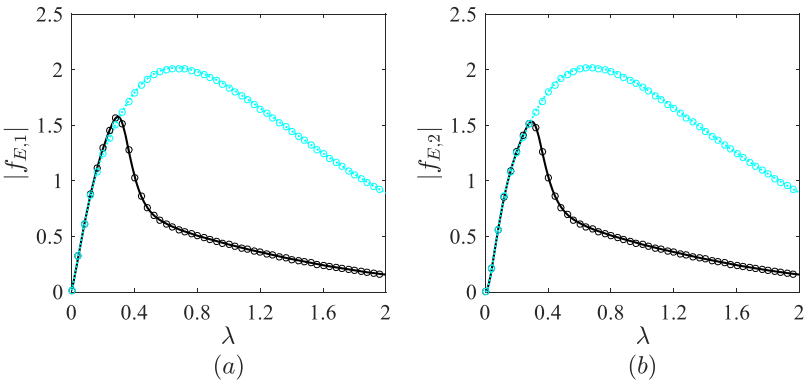


FIG. 4. Wave exciting force on a submerged circular cylinder with a single crack on the left. Solid lines: $c_1 = -10$; dotted lines: ice sheet without crack. Open circles: analytical solutions based on the multipole expansion. ($a = 1$, $b = 1$, $x' = 0$, $z' = -1.2$, $H = 20$, $h = 0.2$, $m = 0.18$, $L = 72.932$).

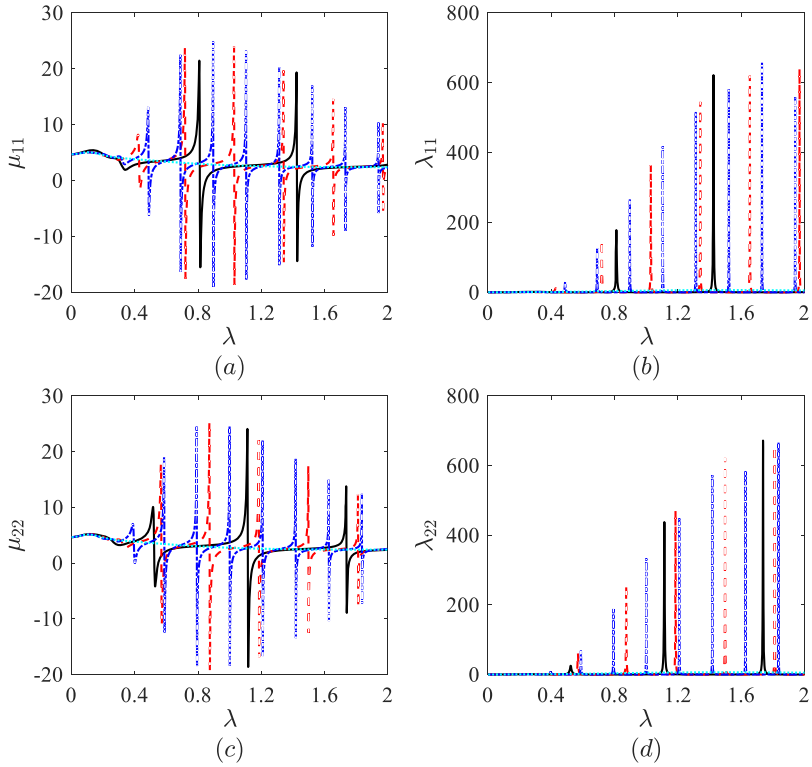


FIG. 5. Hydrodynamic coefficients of a submerged circular cylinder with a crack on its each side. Solid lines: $c_1 = -5$; dashed lines: $c_1 = -10$; dotted-dashed lines: $c_1 = -15$; dotted lines: ice sheet without the crack. ($a = 1$, $b = 1$, $x' = 0$, $z' = -1.2$, $H = 20$, $h = 0.2$, $m = 0.18$, $L = 72.932$).

no visible difference between the present results and those analytical solutions, i.e., the present numerical procedure is accurate.

After the accuracy of the present method has been verified through a single crack, we next consider the case in which two cracks are located symmetrically about the body centre or $c_2 = -c_1$. The hydrodynamic coefficients with $c_1 = -5, -10, -15$ are shown in Fig. 5, while the wave exciting force is provided in Fig. 6. Since the problem is symmetric about $x = 0$, we have $\tau_{kj} = 0$ for odd $k + j$, which are omitted from the figures. When $\lambda$ is very small, we can see from Figs. 5 and 6 that the results for ice sheets with two cracks tend to those without cracks. This is because as $\lambda \to 0$, the condition in Eq. (3) tends to $\partial\phi_j/\partial z = 0$, which means that $\partial^3\phi_j/\partial z\partial x^2 \to 0$ and $\partial^4\phi_j/\partial z\partial x^3 \to 0$ hold on the whole ice sheet, i.e., the crack conditions are satisfied automatically. In such a condition, results for an ice sheet with any number of cracks will then tend to those without crack.

As $\lambda$ increases, it can be seen from these figures that the results for the ice sheet without the crack change smoothly. However, for the case with two cracks, the results show a quite oscillatory behavior. Compared with Fig. 3, we can see in Fig. 5 that the added mass can reach a large peak at some frequencies, which is followed immediately by a negative trough. This can be explained through the approximate solution in Appendix C based on the wide spacing approximation. For a circular cylinder and noticing $c_2 = -c_1$, we can simplify $\varepsilon_j^1$ and $\varepsilon_j^2$ in Eqs. (C2) and (C3) as

$$\varepsilon_j^1 = (-1)^j \varepsilon_j^2 \quad \text{and} \quad \varepsilon_j^2 = \frac{A_j^- R}{e^{+i\lambda l} - [r_0 + (-1)^j t_0]R}, \tag{66}$$

where $A_j^+ = (-1)^j A_j^-$, $t_0 = t_0^- = t_0^+$, and $r_0 = r_0^- = r_0^+$ for a body symmetric about its middle plane have been used.[25] Substituting Eq. (66) into Eq. (C1) and using $f_{E,k}^{\circ -} = 2I\rho\omega Q_0 C_g A_k^-$ and $f_{E,k}^{\circ +} = (-1)^k f_{E,k}^{\circ -}$, we can write $\tau_{kj}$ as

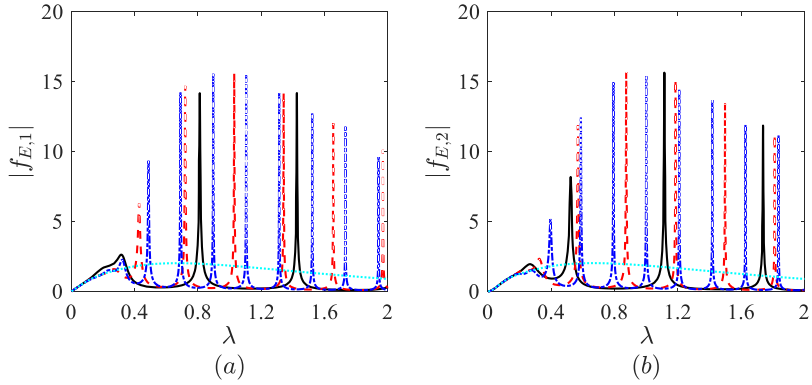


FIG. 6. Wave exciting force on a submerged circular cylinder with a crack on its each side. Solid lines: $c_1 = -5$; dashed lines: $c_1 = -10$; dotted-dashed lines: $c_1 = -15$, dotted lines: ice sheet without the crack. ($a = 1$, $b = 1$, $x' = 0$, $z' = -1.2$, $H = 20$, $h = 0.2$, $m = 0.18$, $L = 72.932$).

$$\tau_{kj} = \tau_{kj}^{o} + 2\mathrm{i}\rho Q_0 C_g\left[(-1)^{k+j}+1\right]A_{kj}, \tag{67}$$

where

$$A_{kj} = \frac{A_k^- A_j^- R}{\mathrm{e}^{+\mathrm{i}\lambda l} - [r_0 + (-1)^j t_0]R}, \tag{68}$$

with

$$Q_0 = \frac{\rho\omega(L\lambda^4+\rho g)}{(L\lambda^4+\rho g - m\omega^2)^2}, \tag{69}$$

$$C_g = \frac{2L\lambda^3\omega}{L\lambda^4+\rho g} + \frac{\omega}{2\lambda}\left[1+\frac{2\lambda H}{\sinh(2\lambda H)}\right]\frac{L\lambda^4+\rho g - m\omega^2}{L\lambda^4+\rho g}. \tag{70}$$

Invoking Eq. (68), we have that when $\delta_\lambda = \lambda l$ equals

$$\delta_e = 2n\pi + \mathrm{Arg}\left\{[r_0 + (-1)^j t_0]R\right\}, \tag{71}$$

$|A_{kj}|$ will reach its peaks. Similar to Eq. (8.6.49) in the work of Mei, Stiassnie, and Yue,[25] we have

$$r_0 + (-1)^j t_0 = -\mathrm{e}^{2\mathrm{i}\mathrm{Arg}(A_j^-)}, \tag{72}$$

which gives

$$|r_0 + (-1)^j t_0| = 1 \quad \text{and} \quad \mathrm{Arg}[r_0 + (-1)^j t_0] = 2\mathrm{Arg}(A_j^-) + \pi. \tag{73}$$

Near $\delta_e$ at each $n$, we may write $\delta_\lambda = \delta_e + \Delta$. Equation (68) becomes

$$A_{jj} \approx |A_j^- A_j^- R|\frac{|R| - \mathrm{e}^{-\mathrm{i}\Delta}}{||R| - \mathrm{e}^{\mathrm{i}\Delta}|^2}, \tag{74}$$

where Eq. (73) has been used. Substituting the above equation into Eq. (67), we have

$$\mu_{jj} \approx \mu_{jj}^{o} - 4\rho Q_0 C_g |A_j^- A_j^- R|\frac{\sin\Delta}{||R| - \mathrm{e}^{\mathrm{i}\Delta}|^2}, \tag{75}$$

$$\lambda_{jj} \approx \lambda_{jj}^{o} + 4\rho\omega Q_0 C_g |A_j^- A_j^- R|\frac{\cos\Delta - |R|}{||R| - \mathrm{e}^{\mathrm{i}\Delta}|^2}. \tag{76}$$

As $\lambda$ increases, we have $|R| \approx 1$, which leads to $||R| - \mathrm{e}^{\mathrm{i}\Delta}| \approx 0$ as $\Delta \approx 0$. Then invoking Eq. (75), we have that the added mass will change from a large positive peak to a large negative trough, through following the sign of $\sin\Delta$, while invoking Eq. (76), we have that the damping coefficient will have a large peak at $\delta_\lambda = \delta_e$, but there will be no sharp variation from the peak to trough due to the term $\cos\Delta$. For the wave exciting force, we can simplify Eq. (C11) as

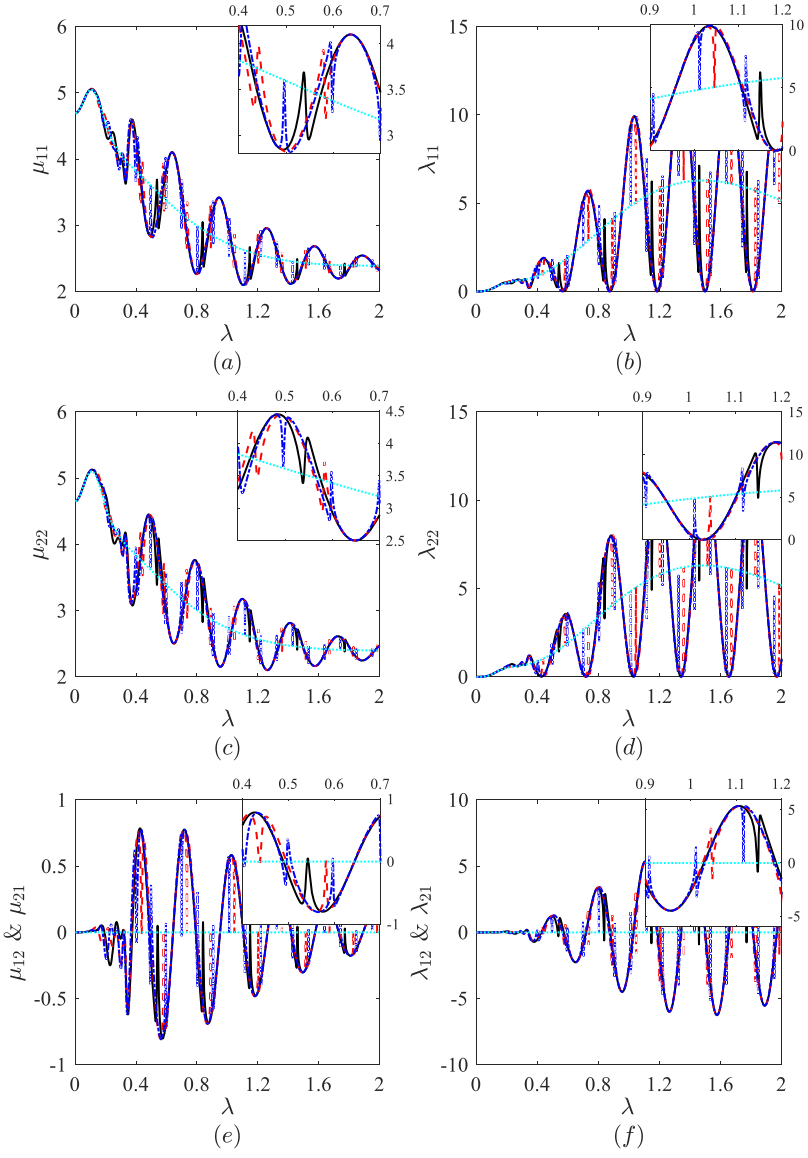


FIG. 7. Hydrodynamic coefficients of a submerged circular cylinder with two cracks on its left side. Solid lines: $c_1 = -20$ and $c_2 = -10$; dashed lines: $c_1 = -30$ and $c_2 = -10$; dotted-dashed lines: $c_1 = -40$ and $c_2 = -10$; dotted lines: ice sheet without the crack. ($a = 1$, $b = 1$, $x' = 0$, $z' = -1.2$, $H = 20$, $h = 0.2$, $m = 0.18$, $L = 72.932$).

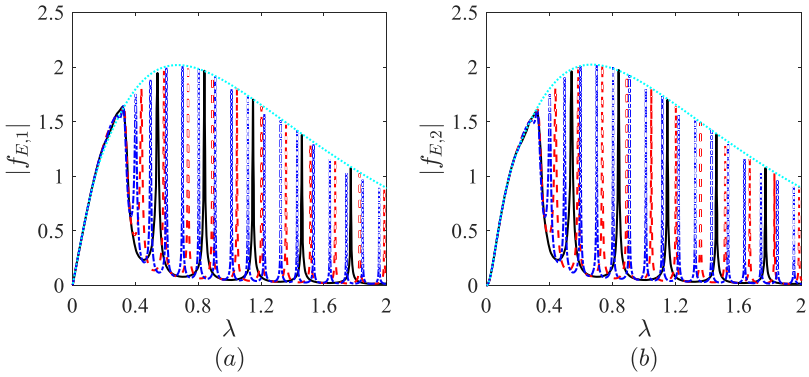


FIG. 8. Wave exciting force on a submerged circular cylinder with two cracks on its left side. Solid lines: $c_1 = -20$ and $c_2 = -10$; dashed lines: $c_1 = -30$ and $c_2 = -10$; dotted-dashed lines: $c_1 = -40$ and $c_2 = -10$; dotted lines: ice sheet without the crack. ($a = 1, b = 1, x' = 0, z' = -1.2$, $H = 20$, $h = 0.2$, $m = 0.18$, $L = 72.932$).

$$f_{E,j} = \frac{f_{E,j}^{\circ -} T e^{+i\lambda l}}{e^{+i\lambda l} - [r_0 + (-1)^j t_0]R}. \tag{77}$$

Then similar to Eq. (68), we can conclude that $|f_{E,j}|$ will have a large peak at $\delta_\lambda = \delta_e$, as can be observed in Fig. 6. It should be noticed that the above discussions are suitable for a body with arbitrary shape, which is symmetric about its middle plane.

In Figs. 7 and 8, we show the results for the case in which both cracks are located on the left side of the body. It can be seen that the hydrodynamic coefficients globally follow the similar oscillations to those in Fig. 3 for a single crack. However, there are also some local oscillations. It may be understood that when the two cracks are located far away from the body, the effect on the body by the wave diffraction by these two cracks could be considered jointly. The result in Eq. (C10) for a single crack can be used in such a case once $R$ for a single crack is replaced by $R_c$ for two cracks. It should also be noted that $R$ in Eq. (C10) corresponds to the incident wave from $x = +\infty$ and the crack at $x = 0$. Accordingly, $R_c$ should correspond to the wave from $x = +\infty$, which encounters the crack at $x = 0$ first and then the crack at $x = c_1 - c_2$. Equation (58) is for the wave from $x = -\infty$, which encounters the first and second cracks at $x = c_1$ and $c_2$, respectively. To use the equation for the current case, we can reverse the wave direction and also the direction of the $x$ axis. Replacing $c_1$ in Eq. (58) with $x = 0$ which is the position of the first crack in the current case, we have

$$R_c = R + \frac{RT^2 e^{-2i\lambda l}}{1 - R^2 e^{-2i\lambda l}}. \tag{78}$$

Then Eq. (C10) can be given as

$$\varepsilon_j^2 = \frac{A_j^- R_c}{e^{-2i\lambda c_2} - r_0 R_c}. \tag{79}$$

Here $c_2$ is used in Eq. (79), as to the body this is the place where the reflection wave is originated. Substituting Eq. (79) into Eq. (C1) and using $f_{E,k}^{\circ -} = 2I\rho\omega Q_0 C_g A_k^-$, we have

$$\tau_{kj} = \tau_{kj}^{\circ} + 2i\rho Q_0 C_g B_{kj}, \tag{80}$$

where

$$B_{kj} = \frac{R_c A_k^- A_j^-}{e^{-2i\lambda c_2} - r_0 R_c}. \tag{81}$$

The above equation indicates that $|B_{kj}|$ will reach its peaks when $\lambda c_2 = n\pi - \mathrm{Arg}(r_0 R_c)/2$. However, for the circular cylinder case, we have $r_0 \approx 0$.[15] Substituting this into Eq. (81), we obtain

$$B_{kj} \approx R_c A_k^- A_j^- e^{+2i\lambda c_2}. \tag{82}$$

Here, we first notice that it does not have the small denominator in $B_{kj}$, which has led to the behavior of the hydrodynamic coefficients of a cylinder between two cracks discussed previously. Then we can see that both the added mass and damping coefficient will oscillate around the corresponding result for the ice sheet without the crack sinusoidally in the form of $e^{+2i\lambda c_2}$, as can be observed in Fig. 3. They also vary with $R_c$ whose denominator can also be small, as can be seen from Eq. (78). At this frequency, $\tau_{kj}$ changes sharply and a spike

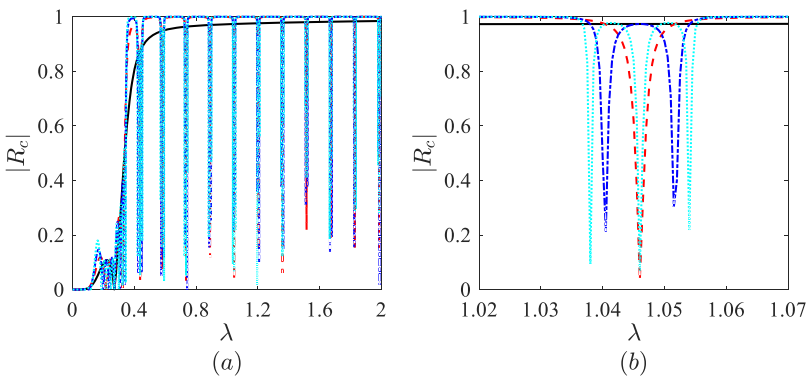


FIG. 9. Reflection coefficient for the wave propagating across the cracks without the elliptical cylinder. Solid lines: $N = 1$; dashed lines: $N = 2$; dotted-dashed lines: $N = 3$; dotted lines: $N = 4$. (b) is the local amplification of (a). ($a = 1, l = 20, H = 20, h = 0.2, m = 0.18, L = 72.932$).

can be observed in Fig. 7. The spike will appear approximately periodically with a period of $\lambda l = \pi$. As discussed in Sec. IV A, there are a series of discrete wave numbers at which $R_c = 0$, indicating that the hydrodynamic coefficients in Eq. (80) will be the same as those for the ice sheet without the crack. For the wave exciting force, the approximation of an equivalent crack can also be used. Substituting Eq. (C15) into Eq. (C11), and replacing $T$ with $T_c$ which is for the wave from $x = -\infty$ and two cracks located at $x = c_1 - c_2$ and $x = 0$, respectively, for the reason discussed above Eq. (78), we have

$$f_{E,k} = f_{E,k}^{\circ-} T_c \frac{e^{-2i\lambda c_2}}{e^{-2i\lambda c_2} - r_0 R_c}, \tag{83}$$

the denominator of which is the same as that of Eq. (81). Similarly, for the circular cylinder case, Eq. (83) can be further simplified as

$$f_{E,k} \approx f_{E,k}^{\circ-} T_c, \tag{84}$$

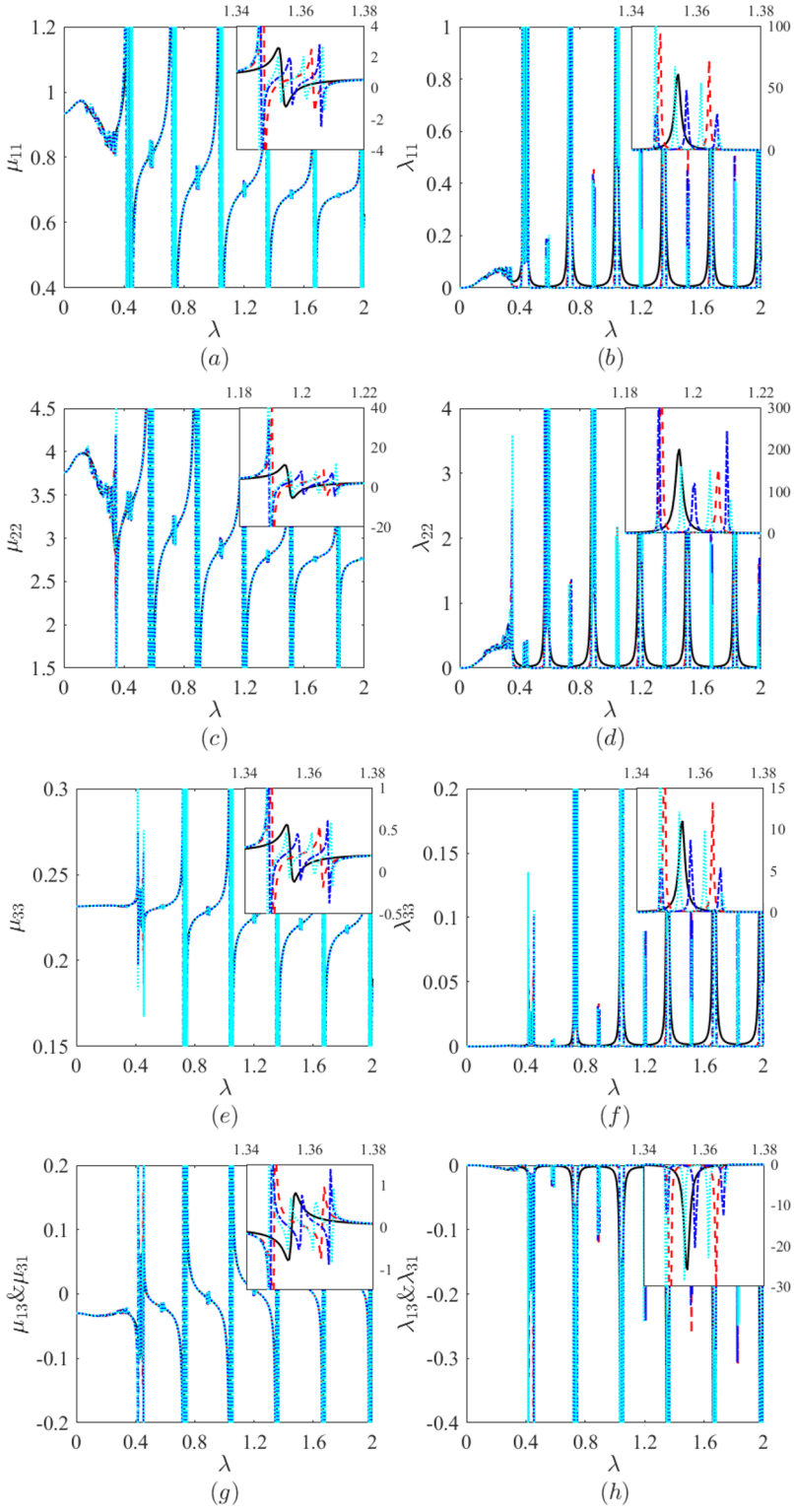


FIG. 10. Hydrodynamic coefficients of a submerged elliptical cylinder with evenly equally distributed cracks. Solid lines: $N = 2$; dashed lines: $N = 4$; dotted-dashed lines $N = 6$; dotted lines: $N = 8$. ($a = 1$, $b = 0.5$, $l = 20$, $x' = 0$, $z' = -1.2$, $H = 20$, $h = 0.2$, $m = 0.18$, $L = 72.932$).

where $r_0 \approx 0$ has been used. In the above equation, $T_c$ can be obtained from Eq. (59) directly. Although Eqs. (58) and (59) are obtained from the wide spacing approximation, $|R_c|^2 + |T_c|^2 = 1$ is satisfied, as $|R|^2 + |T|^2 = 1$. Thus $|T_c| \le 1$, which means that $|f_{E,k}| \le |f^{\circ-}_{E,k}|$, i.e., the wave exciting force here will be always smaller than that on the cylinder submerged below the ice sheet without the crack, apart from at some discrete points where $|T_c| = 1$, which is reflected in Figs. 4 and 8. From Eqs. (58) and (59), we can also find that the denominators of $R_c$ and $T_c$ are the same. Thus the oscillatory behaviors of spikes of the hydrodynamic coefficients in Eqs. (80) and (83) are the same, which can be seen in Figs. 7 and 8.

### C. Body submerged below an ice sheet with multiple cracks

Here we consider the interaction of the wave with a body submerged below an ice sheet with $N$ cracks. The body shape is defined as an ellipse with $b/a = 0.5$. The cracks are evenly distributed with $c_i = -l/2 - (N/2 - i)l$ for $i = 1, \ldots, N/2$. Since both the body and the crack distribution are symmetric about $x = 0$, we have $\tau_{kj} = 0$ for odd $k + j$. The computed added mass and damping coefficient are shown in Fig. 10, against $\lambda$, while in Fig. 11 the wave exciting force is provided, for $N = 2, 4, 6, 8$. It can be seen from these figures that the hydrodynamic coefficients and wave exciting forces for each case all tend to the same value when $\lambda \to 0$, for the reason discussed in Sec. IV B. As $\lambda$ increases, the typical feature of the hydrodynamic forces is oscillation due to that the waves will be continuously reflected between the cracks and the body. It is interesting to see that away from the extremes, the hydrodynamic forces for $N > 1$ are very close to each other, and near the extremes larger $N$ leads to more smaller oscillations. We may use the wide spacing approximation again to analyze the behavior of the results. When the cracks nearest to the body are relatively far away, Eq. (68) can be used provided that $R$ is replaced by $R_c$ due to the wave from $x = +\infty$ and $N/2$ cracks located at $c_i$=$(i - N/2)l$. It becomes

$$A_{kj} = \frac{A^-_k A^-_j R_c}{e^{+i\lambda l} - [r_0 + (-1)^j t_0]R_c}, \tag{85}$$

where $c_{N/2+1} - c_{N/2} = l$ has been used. Similarly, for the same crack distribution as earlier, Eq. (77) can be used, provided that $T$ is replaced by $T_c$ due to the wave from $x = -\infty$,

$$f_{E,j} = \frac{f^{\circ-}_{E,j} T_c e^{+i\lambda l}}{e^{+i\lambda l} - [r_0 + (-1)^j t_0]R_c}. \tag{86}$$

As discussed by Porter and Evans[13] for wave/crack interaction without the body, there exist stopping bands when the incident wave propagates through the semi-infinite array of equally spaced cracks, within which $|R_c| = 1$ and $|T_c| = 0$. For a finite array of cracks, as can be seen in Fig. 9, $|R_c| \approx 1$ within the near stopping bands, and $|R_c|$ has a sharp variation from the near stopping band to the non-stopping band. Each of the non-stopping bands is quite narrow, within which there are more peaks at larger $N$. Within the near stopping bands, the results for different $N$ are then expected to be similar, as $|R_c| \approx 1$ in Eqs. (85) and (86). In the very narrow non-stopping bands, the sharp variation of $R_c$ will lead to additional spikes in Eqs. (85) and (86). As there are more peaks within the narrow non-stopping band at larger $N$, correspondingly, there will be more oscillations in Eqs. (85) and (86) within this band. All these are reflected in Figs. 10 and 11.

Computations are then carried out for odd $N$, which are distributed symmetrically about the body center, i.e.,

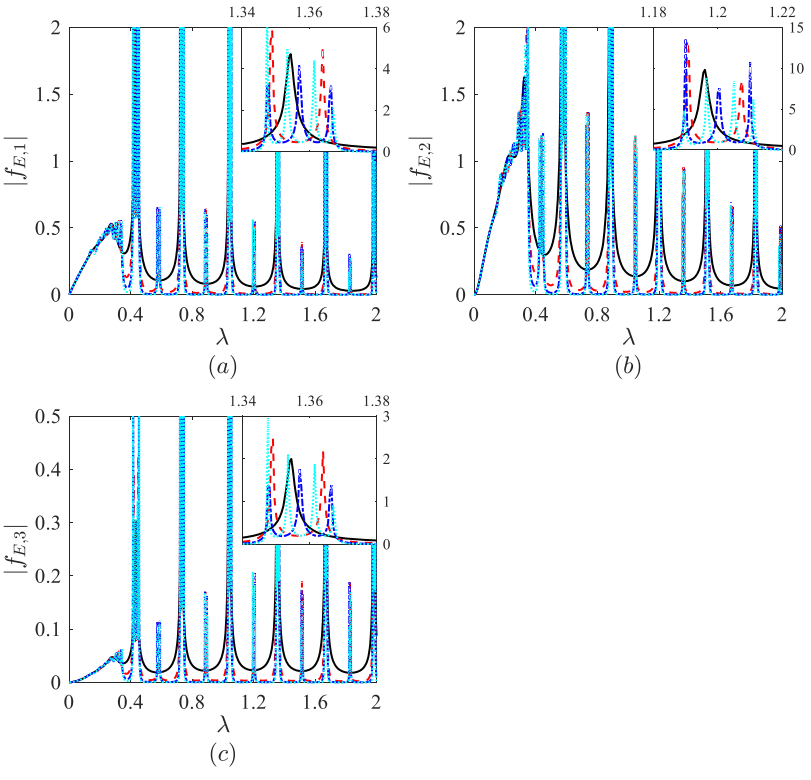


FIG. 11. Wave exciting force on a submerged elliptical cylinder with evenly equally distributed cracks. Solid lines: $N = 2$; dashed lines: $N = 4$; dotted-dashed lines $N = 6$; dotted lines: $N = 8$. ($a = 1$, $b = 0.5$, $l = 20$, $x' = 0$, $z' = -1.2$, $H = 20$, $h = 0.2$, $m = 0.18$, $L = 72.932$).

$c_i = -l/2 - [(N-1)/2 - i]l$ for $i = 1, \ldots, (N-1)/2$ and $c_{(N+1)/2} = 0$. Figure 12 shows the added mass and damping coefficient against $\lambda$, while Fig. 13 gives the results for the wave exciting force. The parameters adopted are the same as those in Figs. 10 and 11, except that there is an additional crack located at the origin. It should be noticed that if we combine the middle crack at the origin and the cylinder as a single problem, then Eqs. (85) and (86) can be used again, provided that $A_j^-$, $r_0$, and $t_0$ are for the cylinder submerged below an ice sheet with a crack at the origin. It may be noted that $R_c$ and $T_c$ in both cases are the same, indicating that the local spikes in Figs. 12 and 13 should be similar to those in Figs. 10 and 11. It may be also noted that Eq. (72) remains valid for the ice sheet with cracks, but the argument of $[r_0 + (-1)^j t_0]$ is different from that for the ice sheet without the crack. From this, we can expect that the large peaks corresponding to $\delta_e$ in Eq. (71) should occur at different $\lambda$, as can be observed through the comparison of Figs. 12 and 13 with Figs. 10 and 11.

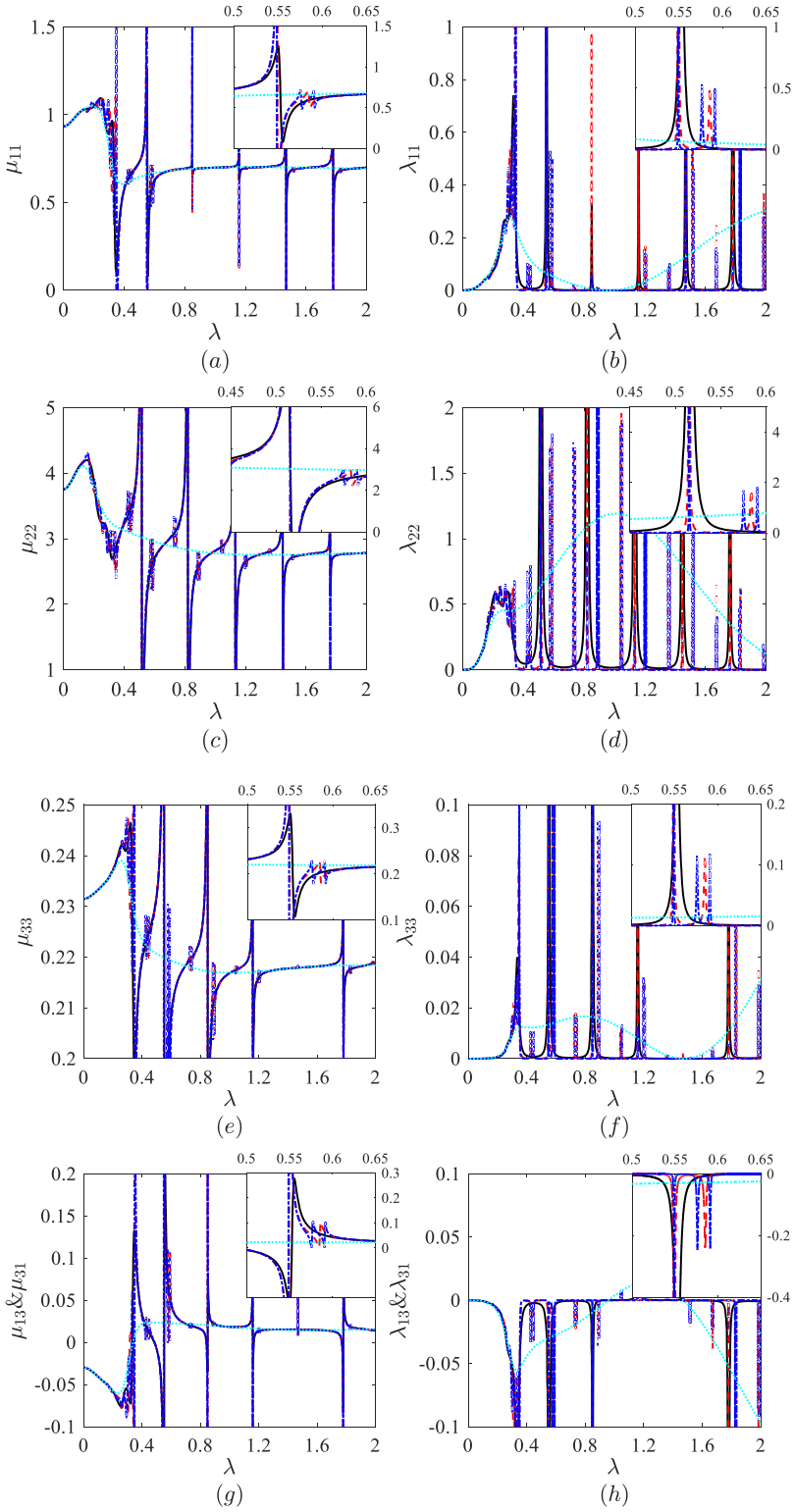


FIG. 12. Similar to Fig. 10, but with an additional crack at the origin. Solid lines: $N = 3$; dashed lines: $N = 5$; dotted-dashed lines $N = 7$; dotted lines: $N = 1$. ($a = 1$, $b = 0.5$, $l = 20$, $x' = 0$, $z' = -1.2$, $H = 20$, $h = 0.2$, $m = 0.18$, $L = 72.932$).

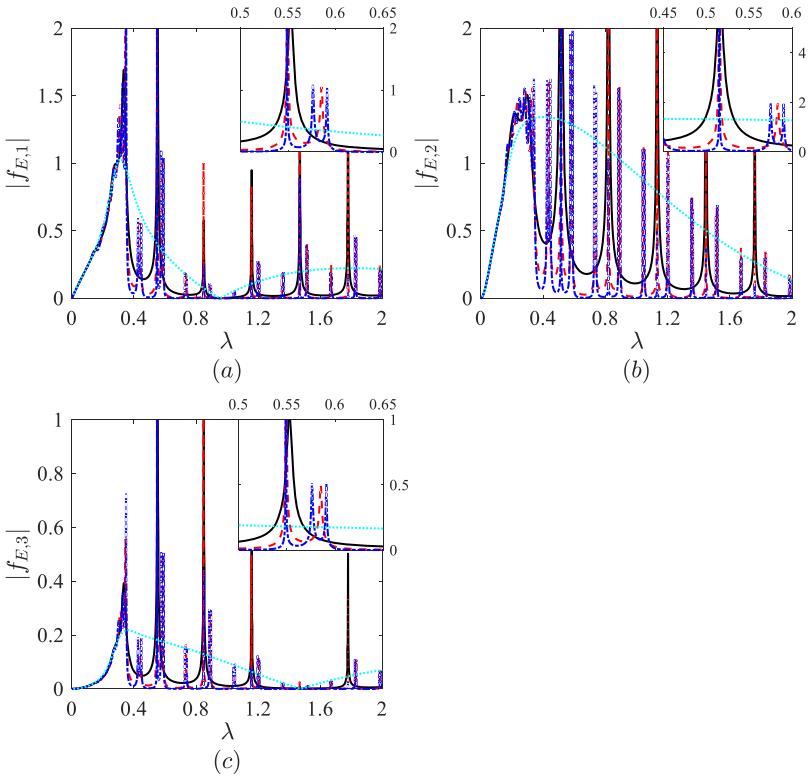


FIG. 13. Similar to Fig. 11, but with an additional crack at the origin. Solid lines: $N = 3$; dashed lines: $N = 5$; dotted-dashed lines $N = 7$; dotted lines: $N = 1$. ($a = 1$, $b = 0.5$, $l = 20$, $x' = 0$, $z' = -1.2$, $H = 20$, $h = 0.2$, $m = 0.18$, $L = 72.932$).

However, it can be seen from Figs. 12 and 13 that the large peaks corresponding to $\lambda \approx 1.47$ in the roll mode disappear. It may be noticed that the large peaks are due to the wave reflection from the cracks, which can be seen as a scattering problem for the body. From the dotted lines in Fig. 13, it can be observed that at $\lambda \approx 1.47$ we have that the wave exciting force in the roll mode is nearly zero when there is a single crack at the origin. This together with Eqs. (C1) and (C11) indicates that at $\lambda \approx 1.47$ we have $\tau_{33} \approx \tau_{33}^{o}$ and $f_{E,3} \approx 0$, as reflected in Figs. 12 and 13, respectively. Similar phenomenon can be also seen in the sway mode at $\lambda \approx 0.96$.

## V. CONCLUSIONS

The solution for the interaction problem of the wave with a body submerged below an ice sheet with multiple arbitrarily spaced cracks has been presented. The procedure starts from the Green function satisfying both the ice sheet and crack conditions, based on which the velocity potentials are solved through the method of source distribution over the body surface only. The problem of wave diffraction by the cracks without the body is solved explicitly by using the derived Green function. The numerical procedure is verified through the comparison with the results from the existing work. Extensive results are provided and analyzed for a submerged cylinder, from which the main conclusions can be drawn as follows:

(1) The derived Green function is an effective approach for the wave diffraction problem by the cracks without the body, and an explicit result can be obtained directly.
(2) For wave interaction with two widely spaced cracks, when the localized evanescent waves are ignored, the deflection of the middle ice sheet between the two cracks is found to be oscillatory with the wave number, and no exact standing wave can be expected within the middle ice sheet. When the space between the two cracks is reduced, the reflection and transmission coefficients will tend to that for a single crack except in a small region near a frequency, where a sharp variation occurs.
(3) For a body submerged below an ice sheet with one crack on its each side, at some specific frequencies, the added mass can reach a large peak which is followed immediately by a negative trough, while at the same frequency the damping coefficient and modulus of the wave exciting force will have large peaks, but there will be no sharp variation from the peak to trough.
(4) For a body submerged below an ice sheet with two cracks on one side, the hydrodynamic coefficients and wave exciting forces will follow similar overall oscillations as those of a single crack. However, there are also some local oscillations in the case of two cracks.
(5) There exist stopping bands when the incident wave propagates through the semi-infinite array of equally spaced cracks without the body. For a finite array of cracks, within the near stopping bands, the reflection coefficients from different numbers of cracks are approximately the same, while within the narrow non-stopping bands, more cracks lead to much more oscillations of the reflection coefficient. These are consistent with those observed by Porter and Evans.[13]
(6) For a body submerged below an ice sheet with multiple cracks distributed symmetrically about the body centre, away from the extremes, the hydrodynamic coefficients and wave exciting forces for the ice sheet with different

numbers of cracks are very close to each other within the stopping bands, and near the extremes, more cracks will lead to much more local smaller oscillations within the non-stopping bands.

The present work is another step forward for the highly complex wave/structure/ice interaction problem. In particular, some new findings have been obtained for bodies below the ice sheet with multiple cracks. However, the Green function was constructed based on the assumption of a homogeneous ice sheet of uniform physical properties. In reality, the variation of the physical properties of the ice sheet in many cases may need to be taken into account. Also, all the boundary conditions are linearized, which is invalid when the surface wave and body motion amplitudes are large, relative to the wavelength and the body dimension. Further work will be undertaken to consider these and other effects to provide reliable results for a wide range of practical problems.

## ACKNOWLEDGMENTS

This work is supported by Lloyd's Register Foundation through the joint centre involving University College London, Shanghai Jiaotong University, and Harbin Engineering University, to which the authors are most grateful. Lloyd's Register Foundation helps to protect life and property by supporting engineering-related education, public engagement, and application of research. This work is also supported by the National Natural Science Foundation of China (Grant Nos. 11472088 and 51709131).

## APPENDIX A: SYMMETRY PROPERTY OF THE GREEN FUNCTION

Assuming that $G^a(x,z;x_0^a,z_0^a)$ and $G^b(x,z;x_0^b,z_0^b)$ are two solutions for the field equation (9) and then applying Green's second identity to them, we have

$$2\pi\left[G^a\left(x_0^b,z_0^b;x_0^a,z_0^a\right)-G^b\left(x_0^a,z_0^a;x_0^b,z_0^b\right)\right]=\int_S\left[G^a\left(x,z;x_0^a,z_0^a\right)\frac{\partial G^b\left(x,z;x_0^b,z_0^b\right)}{\partial n}-G^b\left(x,z;x_0^b,z_0^b\right)\frac{\partial G^a\left(x,z;x_0^a,z_0^a\right)}{\partial n}\right]\mathrm{d}S,\quad(A1)$$

where the fluid boundary $S$ is comprised of the seabed $S_H$, ice sheet $S_I$, and two vertical lines $S_{\pm\infty}$ at $x=\pm\infty$, respectively. Noticing that both $G^a$ and $G^b$ satisfy the boundary conditions in Eqs. (3), (4), (6), and (7), we have that only the integral over the ice sheet will remain on the right hand side of Eq. (A1). According to the condition in Eq. (3), and integrating by parts, Eq. (A1) can be rewritten as

$$2\pi\left[G^a\left(x_0^b,z_0^b;x_0^a,z_0^a\right)-G^b\left(x_0^a,z_0^a;x_0^b,z_0^b\right)\right]=\frac{L}{\rho\omega^2}\sum_{i=1}^{N}\left[\left(\frac{\partial^4G^a}{\partial x^3\partial z}\frac{\partial G^b}{\partial z}-\frac{\partial^3G^a}{\partial x^2\partial z}\frac{\partial^2G^b}{\partial x\partial z}+\frac{\partial^3G^b}{\partial x^2\partial z}\frac{\partial^2G^a}{\partial x\partial z}-\frac{\partial^4G^b}{\partial x^3\partial z}\frac{\partial G^a}{\partial z}\right)_{x=c_i^+}^{x=c_i^-}\right]_{z=0}.\quad(A2)$$

Invoking the crack conditions in Eq. (4), Eq. (A2) further provides

$$G^a\left(x_0^b,z_0^b;x_0^a,z_0^a\right)-G^b\left(x_0^a,z_0^a;x_0^b,z_0^b\right)=0.\quad(A3)$$

This means that for the Green function $G(x,\,z;\,x_0,\,z_0)$, $(x,\,z)$ and $(x_0,\,z_0)$ are exchangeable or $G(x_0,\,z_0;\,x,\,z)=G(x,\,z;\,x_0,\,z_0)$.

## APPENDIX B: THE SOURCE DISTRIBUTION FORMULA FOR THE VELOCITY POTENTIAL

Similar to Eq. (A1), applying Green's second identity to $\phi_j$ and $G$ in Eq. (10), we have

$$2\pi\phi_j(x_0,z_0)=\int_S\left[\phi_j(x,z)\frac{\partial G(x,z;x_0,z_0)}{\partial n}-G(x,z;x_0,z_0)\frac{\partial\phi_j(x,z)}{\partial n}\right]\mathrm{d}S,\quad(B1)$$

where $S=S_H+S_I+S_{\pm\infty}+S_B$ with $S_B$ as the body surface. It may be noticed that when $(x_0,\,z_0)$ is fixed, $G$ satisfies the boundary conditions for varying $(x,\,z)$, and vice versa for fixed $(x,\,z)$ and varying $(x_0,\,z_0)$. Thus $\phi_j(x_0,\,z_0)$ on the left hand side of Eq. (B1) satisfies the ice sheet and crack conditions. Invoking the boundary conditions for $\phi_j$ and $G$, and integrating by parts, Eq. (B1) can be rewritten as

$$2\pi\phi_j(x_0,z_0)=\int_{S_B}\left[\phi_j(x,z)\frac{\partial G(x,z;x_0,z_0)}{\partial n}-G(x,z;x_0,z_0)\frac{\partial\phi_j(x,z)}{\partial n}\right]\mathrm{d}S+\frac{L}{\rho\omega^2}\sum_{i=1}^{N}\left[\left(\frac{\partial^4\phi_j}{\partial x^3\partial z}\frac{\partial G}{\partial z}-\frac{\partial^3\phi_j}{\partial x^2\partial z}\frac{\partial^2G}{\partial x\partial z}+\frac{\partial^3G}{\partial x^2\partial z}\frac{\partial^2\phi_j}{\partial x\partial z}-\frac{\partial^4G}{\partial x^3\partial z}\frac{\partial\phi_j}{\partial z}\right)_{x=c_i^+}^{x=c_i^-}\right]_{z=0}.\quad(B2)$$

Invoking the crack conditions in Eq. (4) for $\phi_j$ and $G$, and using the symmetry property of $G$, Eq. (B2) can be further given as

$$2\pi\phi_j(x_0,z_0)=\int_{S_B}\left[\phi_j(x,z)\frac{\partial G(x_0,z_0;x,z)}{\partial n}-G(x_0,z_0;x,z)\frac{\partial\phi_j(x,z)}{\partial n}\right]\mathrm{d}S,\quad(B3)$$

or exchanging the symbols $(x,\,z)$ and $(x_0,\,z_0)$ for $\phi_j$ and $G$ on both sides of Eq. (B3),

$$2\pi\phi_j(x,z)=\int_{S_B}\left[\phi_j(x_0,z_0)\frac{\partial G(x,z;x_0,z_0)}{\partial n}-G(x,z;x_0,z_0)\frac{\partial\phi_j(x_0,z_0)}{\partial n}\right]\mathrm{d}S.\quad(B4)$$

It may be noticed that in Eq. (B3) the normal derivative and integration are carried out with respect to $(x,\,z)$, while in Eq. (B4) those are carried out with respect to $(x_0,\,z_0)$. In the inner domain bounded by the body surface $S_B$, we introduce a potential $\varphi_j$ which satisfies the Laplace equation and the following boundary conditions:

$$\varphi_j = \phi_j \text{ on } S_B. \tag{B5}$$

Applying Green's second identity to $\varphi_j(x_0, z_0)$ and $G(x, z; x_0, z_0)$, we have

$$0 = \int_{S_B} \left[ \varphi_j(x_0, z_0) \frac{\partial G(x, z; x_0, z_0)}{\partial n} - G(x, z; x_0, z_0) \frac{\partial \varphi_j(x_0, z_0)}{\partial n} \right] \mathrm{d}S. \tag{B6}$$

Subtracting Eq. (B6) from Eq. (B4) provides

$$2\pi\phi_j(x, z) = \int_{S_B} \left\{ \left[ \phi_j(x_0, z_0) - \varphi_j(x_0, z_0) \right] \frac{\partial G(x, z; x_0, z_0)}{\partial n} - G(x, z; x_0, z_0) \left[ \frac{\partial \phi_j(x_0, z_0)}{\partial n} - \frac{\partial \varphi_j(x_0, z_0)}{\partial n} \right] \right\} \mathrm{d}S. \tag{B7}$$

Invoking Eq. (B5), Eq. (B7) can be further written as

$$\phi_j(x, z) = \int_{S_B} \sigma_j(x_0, z_0) G(x, z; x_0, z_0) \mathrm{d}S, \tag{B8}$$

where

$$\sigma_j(x_0, z_0) = \frac{1}{2\pi} \left[ \frac{\partial \varphi_j(x_0, z_0)}{\partial n} - \frac{\partial \phi_j(x_0, z_0)}{\partial n} \right]. \tag{B9}$$

## APPENDIX C: SIMPLIFIED SOLUTIONS FOR ONE CRACK ON EACH SIDE OF THE BODY

For the radiation problem, similar to Eq. (40) in the work of Li, Shi, and Wu,[22] based on the wide spacing approximation, we have

$$\tau_{kj} = \tau^{\circ}_{kj} - \varepsilon^1_j f^{\circ+}_{E,k}/g - \varepsilon^2_j f^{\circ-}_{E,k}/g, \tag{C1}$$

where the superscript o means the results are for the ice sheet without the crack, and + and − in $f^{\circ}_{E,k}$ indicate that the wave exciting force is for the incident wave propagating opposite and along the $x$-axis, respectively. Here

$$\varepsilon^1_j = -\frac{(A^-_j t^-_0 - A^+_j r^-_0) R^2 \mathrm{e}^{\mathrm{i}\lambda(c_1-c_2)} + A^+_j R \mathrm{e}^{-\mathrm{i}\lambda(c_1+c_2)}}{(t^+_0 t^-_0 - r^+_0 r^-_0) R^2 \mathrm{e}^{\mathrm{i}\lambda(c_1-c_2)} - \mathrm{e}^{-\mathrm{i}\lambda(c_1-c_2)} + r^-_0 R \mathrm{e}^{\mathrm{i}\lambda(c_1+c_2)} + r^+_0 R \mathrm{e}^{-\mathrm{i}\lambda(c_1+c_2)}}, \tag{C2}$$

$$\varepsilon^2_j = -\frac{(A^+_j t^+_0 - A^-_j r^+_0) R^2 \mathrm{e}^{\mathrm{i}\lambda(c_1-c_2)} + A^-_j R \mathrm{e}^{\mathrm{i}\lambda(c_1+c_2)}}{(t^+_0 t^-_0 - r^+_0 r^-_0) R^2 \mathrm{e}^{\mathrm{i}\lambda(c_1-c_2)} - \mathrm{e}^{-\mathrm{i}\lambda(c_1-c_2)} + r^-_0 R \mathrm{e}^{\mathrm{i}\lambda(c_1+c_2)} + r^+_0 R \mathrm{e}^{-\mathrm{i}\lambda(c_1+c_2)}}, \tag{C3}$$

with $A^{\pm}_j$, $t^{\pm}_0$, and $r^{\pm}_0$, respectively, being the asymptotic values of the radiation potential $\psi^r_j$ and scattering potential $\psi^{s\pm}_0$ for the ice sheet without the crack or

$$\psi^r_j = A^{\pm}_j \mathrm{e}^{\mp \mathrm{i}\lambda x} \frac{\cosh[\lambda(z+H)]}{\cosh(\lambda H)} \text{ as } x \to \pm\infty (k = 1, 2, 3), \tag{C4}$$

$$\psi^{s+}_0 = \left( \mathrm{e}^{+\mathrm{i}\lambda x} + r^+_0 \mathrm{e}^{-\mathrm{i}\lambda x} \right) \frac{\cosh[\lambda(z+H)]}{\cosh(\lambda H)} \text{ as } x \to +\infty, \tag{C5}$$

$$\psi^{s+}_0 = t^+_0 \mathrm{e}^{+\mathrm{i}\lambda x} \frac{\cosh[\lambda(z+H)]}{\cosh(\lambda H)} \text{ as } x \to -\infty, \tag{C6}$$

$$\psi^{s-}_0 = t^-_0 \mathrm{e}^{-\mathrm{i}\lambda x} \frac{\cosh[\lambda(z+H)]}{\cosh(\lambda H)} \text{ as } x \to +\infty, \tag{C7}$$

$$\psi^{s-}_0 = \left( \mathrm{e}^{-\mathrm{i}\lambda x} + r^-_0 \mathrm{e}^{+\mathrm{i}\lambda x} \right) \frac{\cosh[\lambda(z+H)]}{\cosh(\lambda H)} \text{ as } x \to -\infty. \tag{C8}$$

Here $R$ ($T$) is the reflection (transmission) coefficient for a wave propagating across the crack at the origin. When there is only a single crack on the left side of the body or the crack at $c_2$ is removed, Eqs. (C2) and (C3) become

$$\varepsilon^1_j = 0, \tag{C9}$$

$$\varepsilon^2_j = -\frac{A^-_j R}{r^-_0 R - \mathrm{e}^{-2\mathrm{i}\lambda c_1}}. \tag{C10}$$

For the scattering problem, we have

$$f_{E,k} = \gamma_1 f^{\circ+}_{E,k} + \gamma_2 f^{\circ-}_{E,k}, \tag{C11}$$

where

$$\gamma_1 = -\frac{t^-_0 R T \mathrm{e}^{-\mathrm{i}\lambda(c_1+c_2)}}{(t^-_0 t^+_0 - r^-_0 r^+_0) R^2 \mathrm{e}^{\mathrm{i}\lambda(c_1-c_2)} - \mathrm{e}^{-\mathrm{i}\lambda(c_1-c_2)} + r^-_0 R \mathrm{e}^{+\mathrm{i}\lambda(c_1+c_2)} + r^+_0 R \mathrm{e}^{-\mathrm{i}\lambda(c_1+c_2)}}, \tag{C12}$$

$$\gamma_2 = -\frac{(\mathrm{e}^{-\mathrm{i}\lambda(c_1-c_2)} - r^+_0 R \mathrm{e}^{-\mathrm{i}\lambda(c_1+c_2)}) T}{(t^-_0 t^+_0 - r^-_0 r^+_0) R^2 \mathrm{e}^{\mathrm{i}\lambda(c_1-c_2)} - \mathrm{e}^{-\mathrm{i}\lambda(c_1-c_2)} + r^-_0 R \mathrm{e}^{+\mathrm{i}\lambda(c_1+c_2)} + r^+_0 R \mathrm{e}^{-\mathrm{i}\lambda(c_1+c_2)}}. \tag{C13}$$

When the crack at $c_2$ is removed, the above two equations can be simplified as

$$\gamma_1 = 0, \tag{C14}$$

$$\gamma_2 = -\frac{T\mathrm{e}^{-2\mathrm{i}\lambda c_1}}{r_0^- R - \mathrm{e}^{-2\mathrm{i}\lambda c_1}}. \tag{C15}$$

It should be noticed that the above equations are based on the assumption that the horizontal coordinate of the body centre is zero.


[1] G. Q. Robin, "Wave propagation through fields of pack ice," Philos. Trans. R. Soc., A **255**, 313 (1963).
[2] C. Fox and V. A. Squire, "On the oblique reflexion and transmission of ocean waves at shore fast sea ice," Philos. Trans. R. Soc., A **347**, 185 (1994).
[3] T. Sahoo, T. L. Yip, and A. T. Chwang, "Scattering of surface waves by a semi-infinite floating elastic plate," Phys. Fluids **13**, 3215 (2001).
[4] N. J. Balmforth and R. V. Craster, "Ocean waves and ice sheets," J. Fluid Mech. **395**, 89 (1999).
[5] M. H. Meylan and V. A. Squire, "Finite-floe wave reflection and transmission coefficients from a semi-infinite model," J. Geophys. Res. **98**, 12537, https://doi.org/10.1029/93jc00940 (1993).
[6] M. H. Meylan and V. A. Squire, "The response of ice floes to ocean waves," J. Geophys. Res. **99**, 891, https://doi.org/10.1029/93jc02695 (1994).
[7] H. Chung and C. M. Linton, "Reflection and transmission of waves across a gap between two semi-infinite elastic plates on water," Q. J. Mech. Appl. Math. **58**, 1 (2005).
[8] T. D. Williams and V. A. Squire, "Scattering of flexural-gravity waves at the boundaries between three floating sheets with applications," J. Fluid Mech. **569**, 113 (2006).
[9] M. D. Barrett and V. A. Squire, "Ice-coupled wave propagation across an abrupt change in ice rigidity, density, or thickness," J. Geophys. Res.: Oceans **101**, 20825, https://doi.org/10.1029/96jc01920 (1996).
[10] V. A. Squire and T. W. Dixon, "An analytic model for wave propagation across a crack in an ice sheet," Int. J. Offshore Polar Eng. **10**, 173 (2000).
[11] V. A. Squire and T. W. Dixon, "How a region of cracked sea ice affects ice-coupled wave propagation," Ann. Glaciol. **33**, 327 (2001).
[12] D. V. Evans and R. Porter, "Wave scattering by narrow cracks in ice sheets floating on water of finite depth," J. Fluid Mech. **484**, 143 (2003).
[13] R. Porter and D. V. Evans, "Scattering of flexural waves by multiple narrow cracks in ice sheets floating on water," Wave Motion **43**, 425 (2006).
[14] R. Porter and D. V. Evans, "Diffraction of flexural waves by finite straight cracks in an elastic sheet over water," J. Fluids Struct. **23**, 309 (2007).
[15] Z. F. Li, G. X. Wu, and C. Y. Ji, "Wave radiation and diffraction by a circular cylinder submerged below an ice sheet with a crack," J. Fluid Mech. **845**, 682 (2018).
[16] Z. F. Li, Y. Y. Shi, and G. X. Wu, "Large amplitude motions of a submerged circular cylinder in water with an ice cover," Eur. J. Mech. B/Fluids **65**, 141 (2017).
[17] I. V. Sturova, "Wave generation by an oscillating submerged cylinder in the presence of a floating semi-infinite elastic plate," Fluid Dyn. **49**, 504 (2014).
[18] I. V. Sturova, "The effect of a crack in an ice sheet on the hydrodynamic characteristics of a submerged oscillating cylinder," J. Appl. Math. Mech. **79**, 170 (2015).
[19] I. V. Sturova, "Radiation of waves by a cylinder submerged in water with ice floe or polynya," J. Fluid Mech. **784**, 373 (2015).
[20] K. Ren, G. X. Wu, and G. A. Thomas, "Wave excited motion of a body floating on water confined between two semi-infinite ice sheets," Phys. Fluids **28**, 127101 (2016).
[21] Z. F. Li, Y. Y. Shi, and G. X. Wu, "Interaction of waves with a body floating on polynya between two semi-infinite ice sheets," J. Fluids Struct. **78**, 86 (2018).
[22] Z. F. Li, Y. Y. Shi, and G. X. Wu, "Interaction of wave with a body floating on a wide polynya," Phys. Fluids **29**, 097104 (2017).
[23] J. V. Wehausen and E. V. Laitone, *Surface Waves* (Springer-Verlag, Berlin, 1960).
[24] G. X. Wu, "Second-order resonance of sloshing in a tank," Ocean Eng. **34**, 2345 (2007).
[25] C. C. Mei, M. Stiassnie, and K. P. Yue, *Theory and Applications of Ocean Surface Waves Part 1: Linear Aspects* (World Scientific Publishing Co. Pte. Ltd., 2005).